








Tidal amplification and along-strike process variability in a mixed-energy paralic system prograding onto a low accommodation shelf, Edgeøya, Svalbard

Ingrid Anell¹  | Valentin Zuchuat¹  | Anna Daniela Röhnert² | Aleksandra Smyrak-Sikora³  | Simon Buckley⁴  | Gareth Lord³ | Harmon Maher⁵ | Ivar Midtkandal¹  | Kei Ogata⁶  | Snorre Olaussen³ | Per T. Osmundsen⁷ | Alvar Braathen¹ 

¹Department of Geosciences, University of Oslo, Oslo, Norway

²Faculty of Geosciences, Universität Bremen, Bremen, Germany

³Department of Arctic Geology, UNIS—The University Centre in Svalbard, Longyearbyen, Norway

⁴NORCE Norwegian Research Centre AS, Bergen, Norway

⁵Geography and Geology Omaha, University of Nebraska Omaha, Omaha, NE, USA

⁶Dipartimento di Scienze della Terra, dell'Ambiente e delle Risorse (DiSTAR), Università degli Studi di Napoli Federico II Ringgold standard institution, Napoli, Italy

⁷Department of Geoscience and Petroleum, NTNU, Trondheim, Norway

Correspondence

Ingrid Anell, Department of Geosciences, University of Oslo, Norway.
Email: ingrid.anell@gmail.com

Funding information

Norges Forskningsråd, Grant/Award Number: 234152

Abstract

The study describes the depositional development and sediment partitioning in a prograding paralic Triassic succession. The deposits are associated with the advance of large prism-scale clinoforms across a shallower platform area. Approaching the platform, the limited accommodation and associated relative higher rates of deposition generated straighter clinoforms with lower foreset angles. The vertical restriction across the platform is interpreted to have amplified the tidal signature. Sediment was redistributed from the coast into increasingly sandy delta-front deposits, compared to offshore equivalents. The deposits comprise extensive compound dune fields of amalgamated and increasingly clean sandbodies up-section. Rapid deposition of significant amounts of sand led to differential subsidence and growth-faulting in the delta front, with downthrown fault blocks further amplifying the tidal energy through funnelling. A mixed-energy environment created along-strike variability along the delta front with sedimentation governing process-regime. Areas of lower sedimentation were reworked by wave and storm-action, whereas high sedimentation rates preserved fluvially dominated mouth bars. A major transgression, however, favoured tidally dominated deposits also in these areas, attributed to increasing rugosity of the coastline. Formation of an extensive subaqueous platform between the coast and delta front dampened incoming wave energy, and tidally dominated deposits dominate the near-shore successions. Meanwhile formation of wave-built sand-bars atop the platform attest to continued wave influence. The strong tidal regime led to the development of a heterolithic near-shore tidally dominated channel system, and sandier fluvial channels up-river. The highly meandering tidal channels incising the subaqueous platform form kilometre wide successions of inclined heterolithic stratification. The fluvially dominated channels which govern deposition on the delta plain are narrower and slightly less deep, straighter, generally symmetric and filled with

This is an open access article under the terms of the Creative Commons Attribution License, which permits use, distribution and reproduction in any medium, provided the original work is properly cited.

© 2020 The Authors. Basin Research published by International Association of Sedimentologists and European Association of Geoscientists and Engineers and John Wiley & Sons Ltd

cleaner sands. This study provides important insight into tidal amplification and sand redistribution during shallowing on a wide shelf, along with along-strike process-regime variability resulting from variations in sediment influx.

1 | INTRODUCTION

The processes forming clinoforms at various scales and the distribution of sediment within these different systems are fundamental aspects of sedimentology (e.g. Anell & Midtkandal 2017; Bullimore, Henriksen, Liestøl, & Helland-Hansen, 2005; Helland-Hansen & Hampson, 2009; Patruno, Hampson, Jackson, & Dreyer, 2015; Pirmez, Pratson, & Steckler, 1998; Plink-Björklund, 2008; Steel & Olsen, 2002), much of which remains to be fully understood. The study of extensive outcrops provides comprehensive and detailed overview of the lateral and vertical changes in a depositional system, the scale and architecture of sandbodies and the overall temporal and spatial variability of sedimentary facies and depositional environments.

The Triassic sedimentary succession on the Northern Barents Shelf reflects the progressive infill of accommodation by a vast deltaic system advancing from the southeast (Anell, Braathen, & Olaussen, 2014a; Fleming et al., 2016; Glørstad-Clark, Birkeland, Nystuen, Faleide, & Midtkandal, 2011; Høy & Lundschieen, 2011; Riis, Lundschieen, Høy, Mørk, & Mørk, 2008). In the east, the North and South Barents Sea Basins subsided under kilometres-thick Triassic westward thinning deposits. Across the western platform depositional geometries are characterized by north-westward prograding clinoforms. Seismic data offshore highlight a 600–800-m high, prograding, sigmoidal shelf-prism scale set of Triassic clinoforms (C-C', Figure 1; Anell, Braathen, & Olaussen, 2014; Anell, Faleide, & Braathen, 2016; Anell, Lecomte, Braathen, & Buckley, 2016). As this north-westward advancing system approached Edgeøya, which formed part of the Triassic Svalbard Platform, the geometries of the seismic reflectors change towards wedging, very low-angle linear reflectors (B-B', Figure 1), revealing a marked change in depositional character. The shelf-prism system consists of seismic-scale clinoforms built by sediment supplied by smaller-scale deltaic systems which advanced and retreated over the topset area, periodically forming shelf-edge deltas discharging sediment directly to the slope (Johannessen & Steel, 2005; Plink-Björklund, Mellere, & Steel, 2001). Meanwhile the system approaching Edgeøya is of a similar scale to the largest deltaic sized clinoforms (Patruno, Hampson, & Jackson, 2015). It is inferred that the shallower setting prevented the formation of shelf-prism clinoforms, which were instead replaced by a large delta-scale equivalent. The study area on Edgeøya (Figure 1a), provides a stunning kilometres-long outcrop that is optimally located

Highlights

- Tidal amplification across a structural high increased sand deposition in delta front
- Mixed-energy process-regime attributed to variations in influx
- Variations in tidal versus fluvial channel size, fill and geometry recorded
- Changes in clinoform scale and geometries across structural high

to better understand depositional processes in a prograding delta system and changes in the process-regime, sedimentary transport and deposition as it advanced across a shallower platform region. The study provides insight on the northern Barents Shelf, as well as broad implications for structural influence on fluvio-marine processes in analogue settings.

Our study addresses how changes in shallow marine processes impact a prograding succession of clinoforms, merging from shelf-prism to deltaic scale across a structural high. We furthermore use our interpretations to characterize the types and quality of sandstone bodies in terms of reservoir characterization and discuss the depositional environment of the system in relation to the regional development of the Barents Sea.

2 | GEOLOGICAL SETTING

The Barents Shelf consists of numerous sub-platforms, highs and basins that record a long and diverse geological history comprising several major orogenic events and extended periods of rifting (Anell, Faleide, et al., 2016; Anell, Lecomte, et al., 2016; Faleide et al., 2008, Faleide et al., 2008; Gernigon et al., 2014; Henriksen et al., 2011; Johansen et al., 1993; Nøttvedt et al., 1993; Skogseid et al., 2000). At present the Shelf forms a shallow platform whose western edge constitutes the sheared rift-margin to the spreading North Atlantic, and a marked rifted transition to the north into the Eurasian Basin. The southern and eastern limits are comprised by the Scandinavian landmasses and the island of Novaya Zemlya respectively. The Svalbard archipelago lies in the northwest corner, and represents a tilted and uplifted part of the Barents Shelf. This exhumation generates a regional monocline from

north to south, which details an almost complete stratigraphic record from the Paleoproterozoic through Cenozoic. The exposures reflect the Silurian-Devonian Scandian phase of the

Caledonian orogeny (Braathen et al., 1999; Faleide et al., 2018; Gee, Bogolepova, & Lorenz, 2006; Johansson, Gee, Larionov, Ohta, & Tebenkov, 2005; McKerrow, Mac Niocaill,

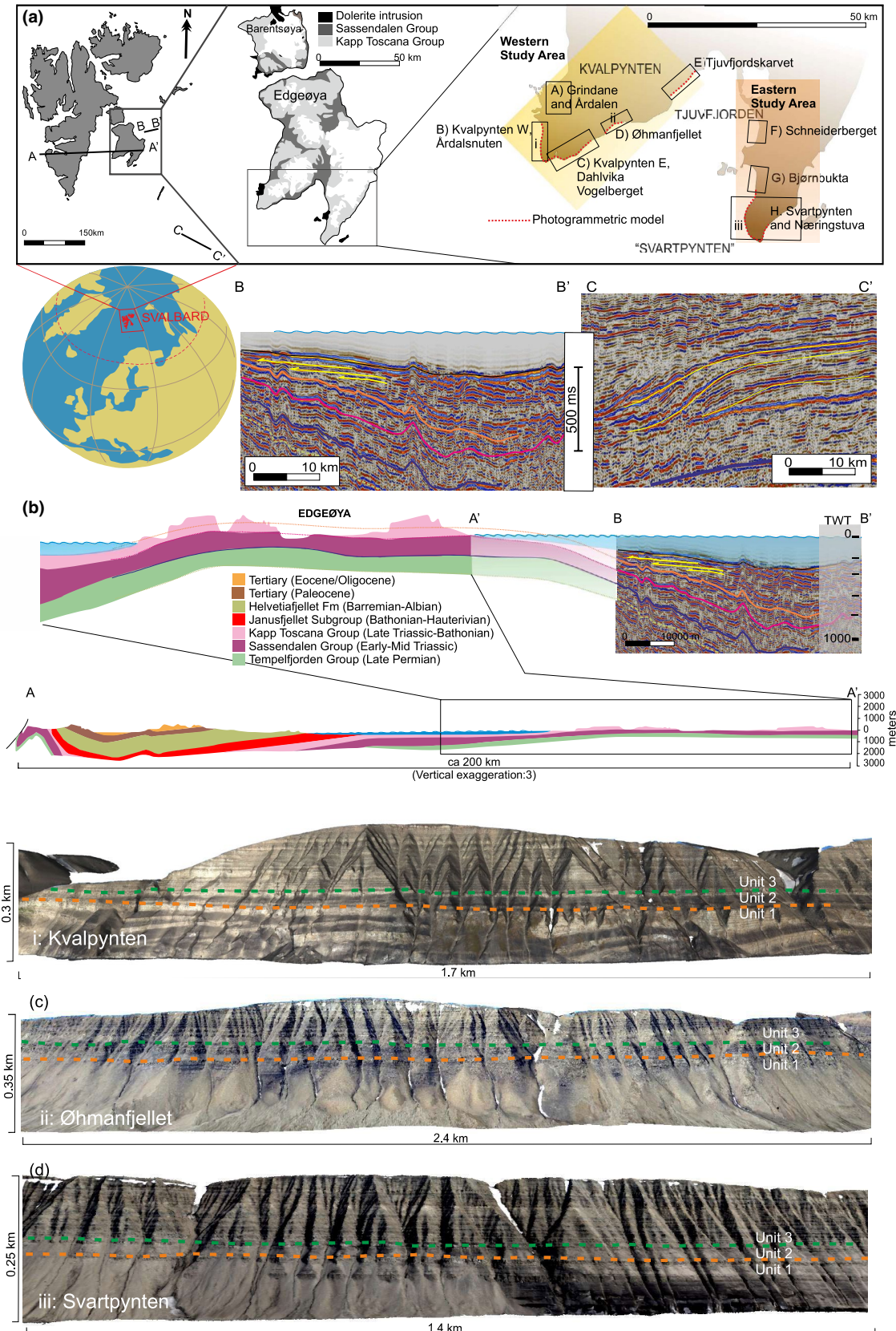


FIGURE 1 (a) Location of the study area including a basic geological map of Edgeøya and Barentsøya redrawn from Sigmond (1992). The close-up of western Edgeøya shows the study area and the subdivision into the west and east study areas and the subareas within these. The stippled red line shows the photogrammetric model coverage. The map on the right shows the location of the location of three transects, A-A' is redrawn from Dallmann, Ohta, Elvevold, and Blomeier (2002) showing the distribution of geological formations in cross-section across Svalbard and the approximate ties to the offshore seismic data. The seismic images (courtesy of the NPD) are figures adapted from Anell, Braathen, et al., 2014; Anell, Faleide, et al., 2016; Anell, Lecomte, et al., 2016) showing the larger sigmoidal clinoform geometries in C-C' and the low-angle tangential clinoforms near Edgeøya on B-B'. The purple marker is the near-base Triassic reflector. The orange reflector has been shown to likely correlate approximately to the faulted to non-faulted transition onshore (Anell, Faleide, et al., 2016; Anell, Lecomte, et al., 2016). The lowermost three figures (b–d) display cliff-sections from the photogrammetric models and the subdivision of the sedimentary units with the colour-coded lines used throughout. The exact correlation to Øhmanfjellet (8b) and Svartpynten (c) is tentative and based on the similarities in sedimentary features and thickness

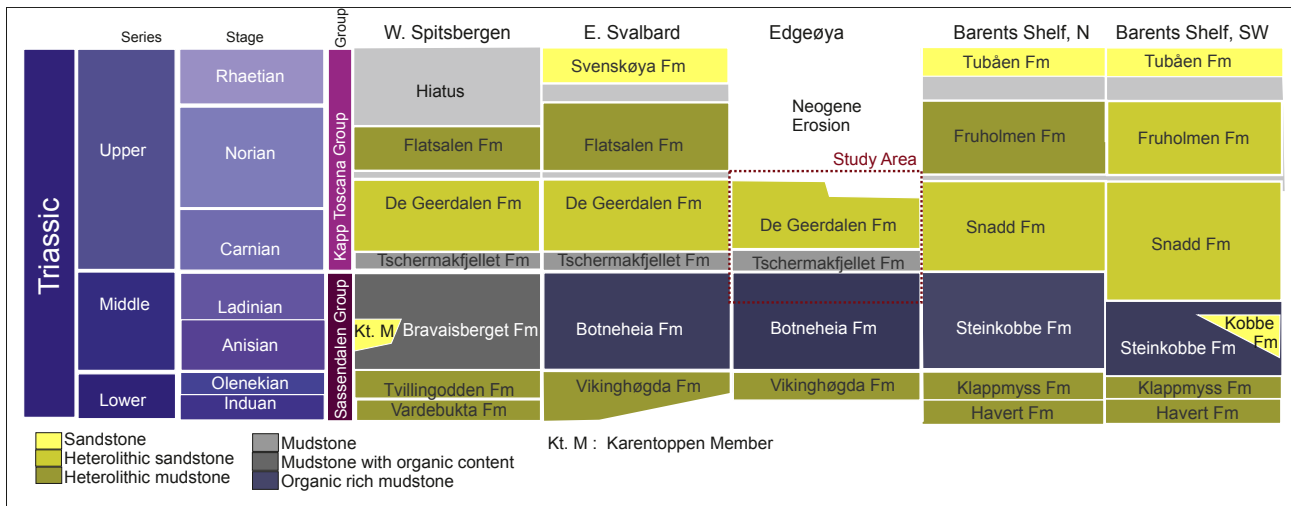


FIGURE 2 Lithostratigraphy of the Triassic to Early Jurassic Barents Sea succession, based on Mørk et al. (1999), Smelror, Petrov, Larssen, and Werner (2009), Mueller, Veld, Nagy, and Kürschner (2014), Vigran, Mangerud, Mørk, Worsley, and Hochuli (2014) and Paterson and Mangerud (2017)

& Dewey, 2000) which sutured Baltica and Laurentia, and was followed by Devonian late/post-orogenic extension and transtension with deposition in supra-detachment basins (Braathen, Osmundsen, Maher, & Ganerød, 2018). Rifting in the Upper Carboniferous–Lower Permian is reflected in thick carbonate deposits, which transitioned to clastic in the latest Permian at the onset of a stable platform (Stemmerik & Worsley, 2005; Worsley, 2008). Platform stability was disturbed by rifting events (late Permian/Early Triassic; early Jurassic/early Cretaceous) that especially dominated the western Barents Shelf, culminating in the Eocene opening of the Norwegian–Greenland Sea (Faleide et al., 2008).

Edgeøya is an island in the south-eastern part of the Svalbard archipelago, where the 300–400 m high cliffs expose a succession of Ladinian–Carnian Triassic outcrops. This succession documents the passage of a large delta-system prograding across the Barents Shelf. The study area (Figure 1a) is located along the south-western coast of the island. The organic-rich, cliff-forming calcareous shales of the Ladinian Blanknuten Member (Mørk et al., 1999) are in places exposed, although most often the lowermost succession consists of the pre-deltaic

shales of the Carnian Tschermakfjellet Formation (Figures 2 and 3). The first sandstones to occur above these shales define the transition to the paralic De Geerdalen Formation, which comprises the remaining parts of the exposed succession. The De Geerdalen Formation records the progressive infill of the Barents Shelf by prograding deltaic systems, which advanced from the southeast (Anell, Braathen, et al., 2014; Anell, Faleide, et al., 2016; Anell, Lecomte, et al., 2016; Glørstad-Clark et al., 2011; Glørstad-Clark, Faleide, Lundschie, & Nystuen, 2010; Høy & Lundschie, 2011; Riis et al., 2008). The lowermost exposures in the De Geerdalen Formation are heavily growth-faulted, and several wedge-shaped coarsening upward units separated by thick shales, fill in associated half-graben basins (Edwards, 1976; Ogata et al., 2018; Osmundsen, Braathen, Rød, & Hynne, 2014; Smyrak-Sikora et al., 2019).

3 | METHODS AND DATA

The dataset comprises over 40 sedimentary logs from various locations between Kvalpynten and Svartpynten (Figure 1)

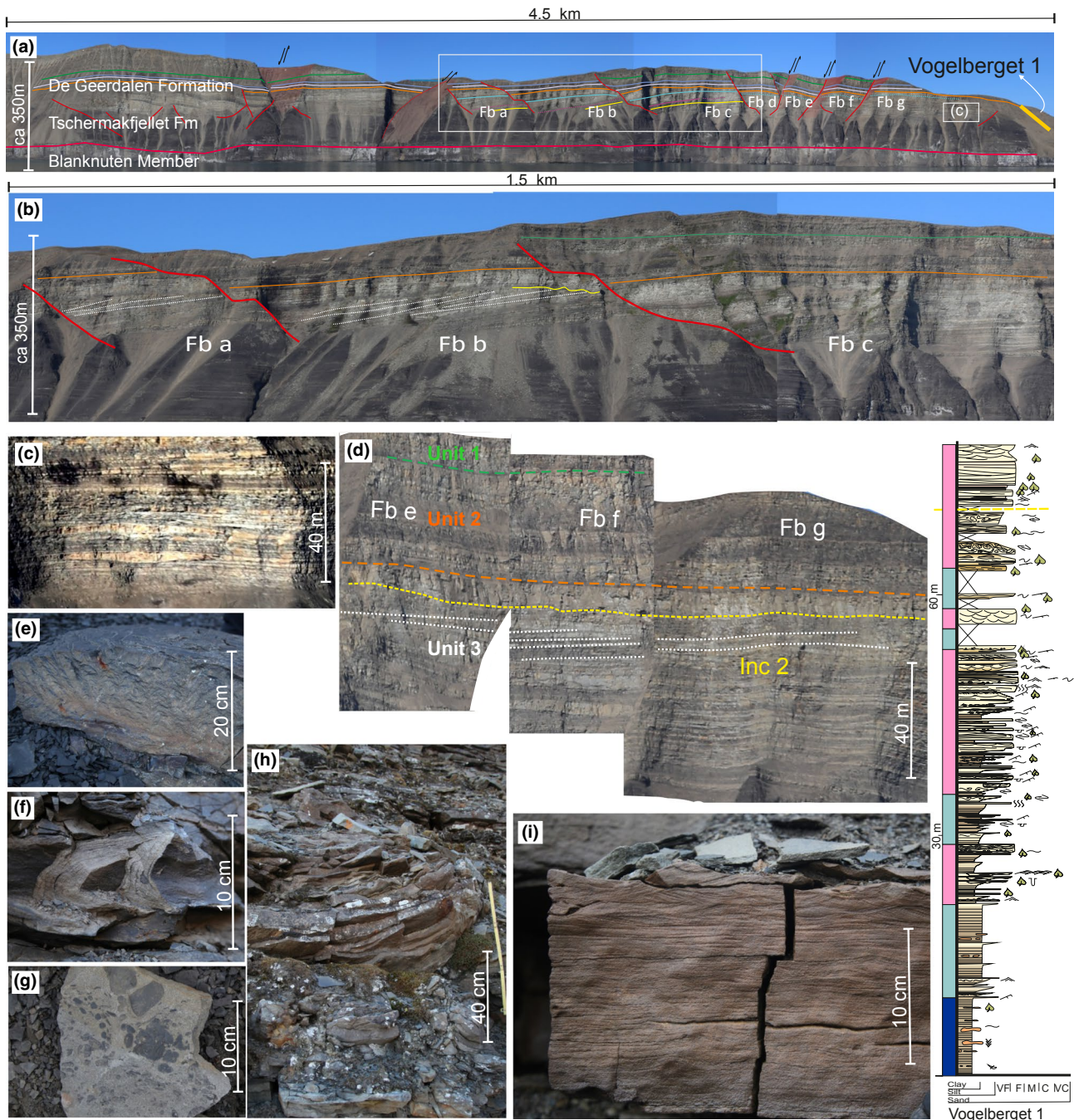


FIGURE 3 The Vogelberget section with the Vogelberget 1 log showing (a) the outcrop of the Blanknuten Member (pink marker) and the fault blocks (fb) in Unit 1. (b and d) show examples of inclined heterolithic strata in mouth bars with (d) showing the erosive, massive sandstone cap overlying the inclined succession. (c) Example of the small sand-lenses observed in this section, location in photogrammetric model in the upper figure. (e) Cone-in-cone structures, (f) small-scale slump folds and (h) large-scale slumped intervals typical for FA 2.1. (g) Mud-chips prevalent in the delta front and (i) red coloured wave-rippled rock marking the upper shoreface

collected during four field-seasons (2012–2015). Out of these, 16 logs were selected to provide the main basis for correlation and interpretation, based on their quality, location and length (Figures 4 and 5). Photogrammetric 3D virtual outcrop models were constructed using georeferenced digital photographs taken from a boat sailing ca. 1–2 km from the outcrop. The photographs were processed using © Agisoft photoscan to provide

a high-density 3D point cloud, which was then triangulated to create a continuous, textured surface model (Figure 6; Buckley, Howell, Enge, & Kurz, 2008; Hodgetts, 2013; Rittersbacher, Howell, & Buckley, 2014). Since the photographs were taken from sea level, their resolution becomes poorer further up-section. Meanwhile, resolution of details in the lowermost cliff-sections can observed features down to 20 cm size. The

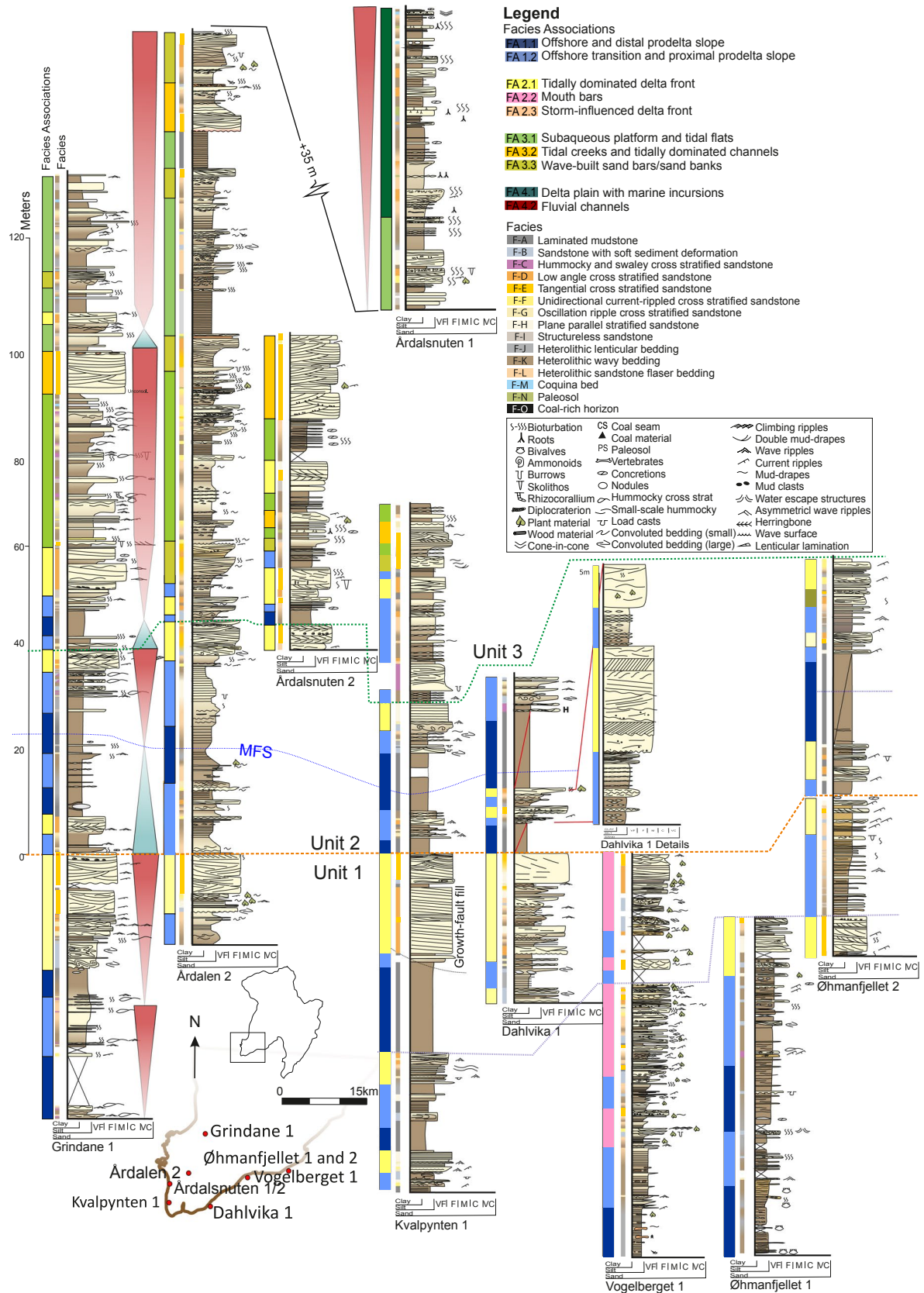


FIGURE 4 Logs from the western study area with colour bars displaying the facies and facies association (see legend) to the left of the logs. The colour markers correspond to the unit subdivision as shown in Figure 1

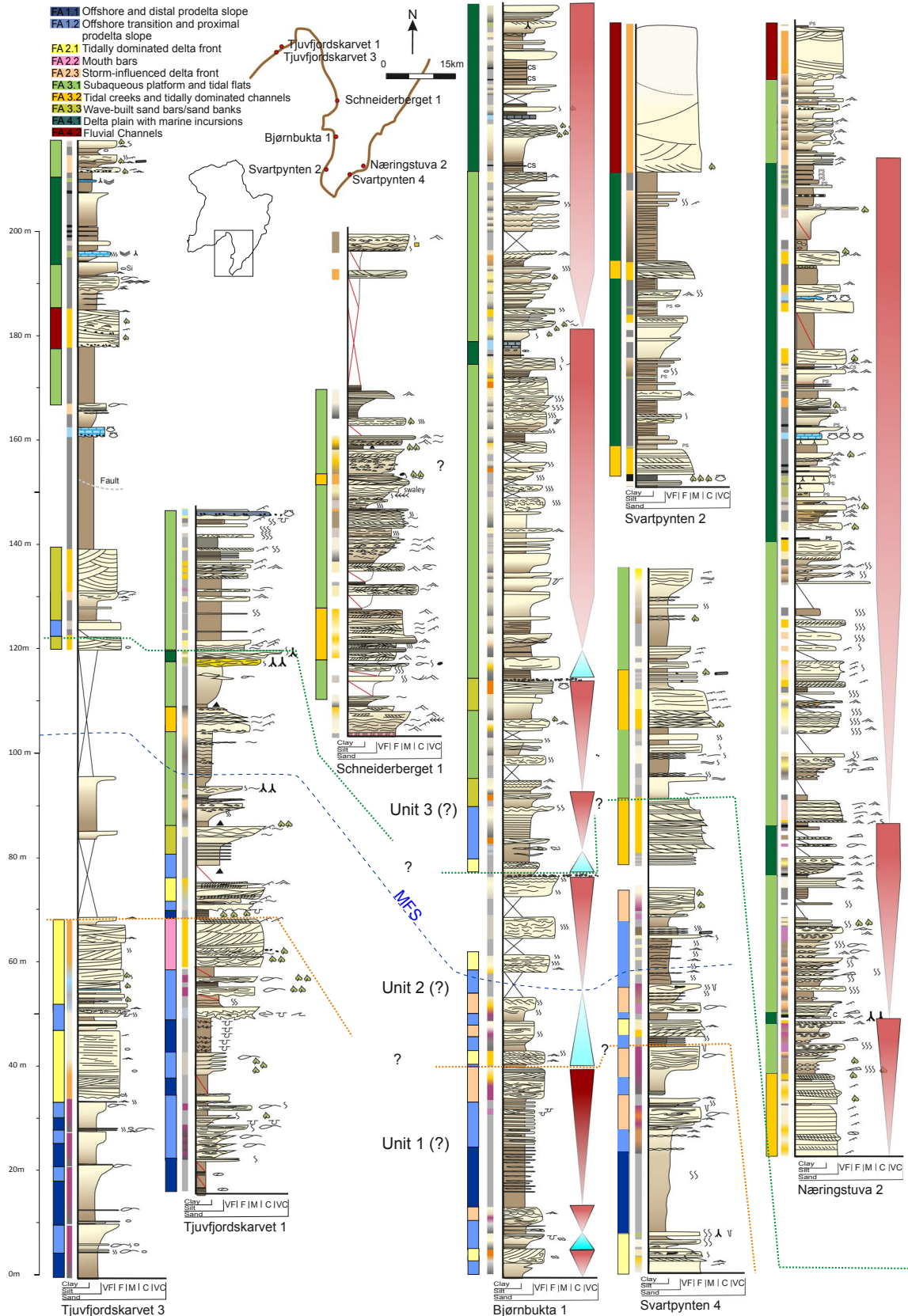


FIGURE 5 Logs in the eastern study area. Facies (Table 1– see colour codes in Figure 4) and Facies association (see legend) are displayed to the left of each log. Probable unit subdivision correlating to Figure 4 is shown with stippled lines

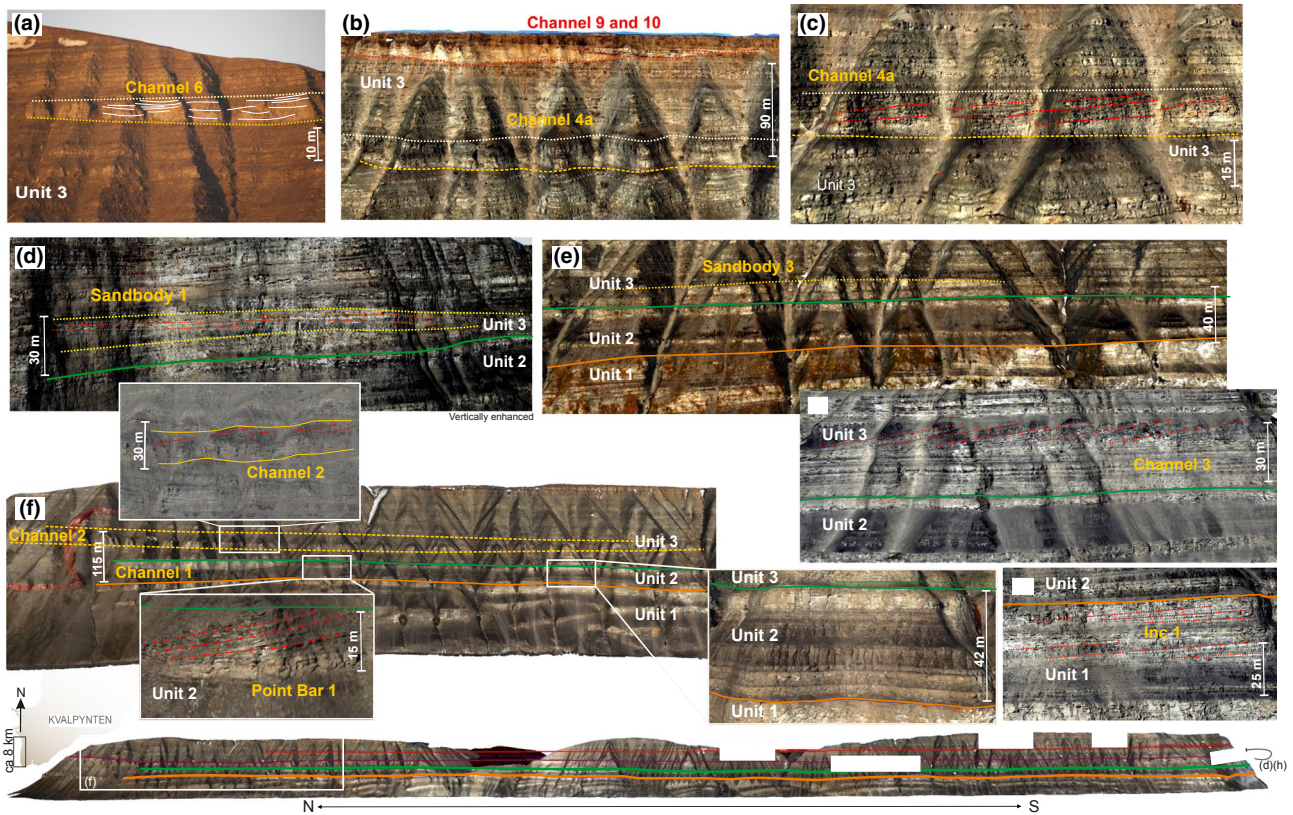


FIGURE 6 Examples of the expression of sand-bodies in photogrammetric model (for details see Table 3). The N-S section at the bottom shows the location of the displayed features. (a) A trough cross-stratified Channel (6 in Table 3) in Unit 3 (b) Stacked offsets of fluvial channels in the uppermost part of the cliff-face (Channels 9 and 10) and below a tidally dominated channel (4a) which can be followed along the whole section (Channels 4 a-c, Table 3) (c) Details of tidally dominated channel 4a showing a trough cross-stratified base fining upward into IHS. (d) Located in Kvalpynten E (around the corner from the section shown along the base) Sandbody 1 shows coarsening upward and displays clear lateral accretion surfaces accreting NNE dipping ca 8°. (e) Sandbody 3 is a convex up massive sandstone with well-expressed dipping flanks dipping NE-SW. (f) A large section of the photogrammetric model which shows the extent of Channel 1 (with details of the point bar in the enlarged image) and Channel 2 which has a strongly erosional base and fines upward to a very muddy point bar which accretes towards the NW, details in the enlargement. The small enlargement to the right displays details of Unit 2 with the two coarsening upward units near the base and a thick mud-dominated succession in the middle of the Unit. (g) Channel 3 which is strongly erosional and displays large IHS dipping ca 12° accreting NW. (h) Inclined 1 (Inc 1, Table 3), located around the corner of the section displayed at the base, shows a stacked succession of prograding coarsening upward units similar to those seen at Vogelberget interpreted to display more classic mouth bars. The two units prograde W/SW

model altogether covers a section length of ca. 45 km around Kvalpynten, Vogelberget, Øhmanfjellet, Tjuvfjordskarvet and Svartpynten (Figure 1a). However, poorer outcrop exposure makes it very difficult to discern much detail outside the western study area (Figure 1c,d). Thus, the work is focused on the details around Kvalpynten and Vogelberget (Figure 1a,b).

LIME software (Buckley et al., 2019) was used for interpretation of the photogrammetric model (Figure 6) to digitize lines and subdivide the succession, make measurements of length and height of units and sand-bodies, observe small and large-scale geological features, infer sequence stratigraphic development and measure bedding orientations. Due to the gentle inclination, measurements were not corrected for the tilt of the whole succession, which creates minor errors in the lowest dipping measurements. The observations and measurements from LIME

were then combined with the sedimentary facies associations interpreted from logged sections.

4 | RESULTS

4.1 | Study areas

The Triassic succession on southwest Edgeøya was assessed in two main study areas, west and east. The western study area is subdivided into five subareas (A-E). These are: (A) Årdalen and Grindane, (B) Kvalpynten including Årdalssnuten, (C) Western Kvalpynten and Vogelberget, (D) Øhmanfjellet and (E) Tjuvfjordskarvet. The eastern study area comprises (F) Schneiderberget, (G) Bjørnbukta, and (H) Svartpynten and Næringstuva (Figures 1,4,5).

TABLE 1 Facies descriptions of the studied section of the Tschermakfjellet and De Geerdalen Formation on Edgeøya

Facies descriptions		
Facies	Description	Grain size Interpretation
A	Laminated (platy) mudstone	Md-Si Deposition from suspended load within a low-energy environment, weak bottom currents may occur locally, as testified by the discrete undulations and rare thin ripple cross-laminations occurring within the mudstone
B	Sandstone with soft sediment deformation	VF-F Soft sediment deformations can occur when an applied stress exceeds the normal yield strength of the sediments or when this yield strength is brutally reduced, notably by liquification, and require to be coupled with a deviatoric stress impacting layers of contrasting density, often reflecting water escape and gravitational (slump) processes (Owen, 1987)
C	Hummocky and swaley cross-stratification	VF-uF Hummocky- (HCS) and swaley (SCS) cross-stratification are generally interpreted to reflect a shallow marine storm-induced oscillatory current (Cheel & Leckie, 1993). Superimposed scattered unidirectional-current ripples illustrate the presence of a weak unidirectional flow from when HCS processes wane. HCS is thought to occur mainly near the Storm-Weather-Wave-Base (SWWB) while SCS represents a shallower depositional setting, between the SWWB and the Fair-Weather-Wave-Base (FWWB; Dumas & Arnott, 2006). Plant fragments indicate a proximal location of the deposits within the system
D	Low-angle cross-stratified sandstone	uVF-uF Low-angle cross-stratification can occur in various depositional setting as transitional bedform between dunes and upper plane beds as flow velocity increases or as sediment concentration in the water increases (Massari, 1996), or between upper plane beds and HCS, as strong oscillatory currents wax (Dumas & Arnott, 2006; Quin, 2011). The presence of scattered oscillation ripples illustrates the impact of minor wave activity over the area. Plant fragments indicate a proximal position of the deposits within the system
E	Tangential cross-stratified sandstone	uVF-M Tangential cross-stratification results from trains of mature 3-D dunes migrating on top of each other under non-laminar unidirectional current (Allen, et al., 1982, Venditti, Church, & Bennett, 2005). Their internal complexity (troughs and reactivation surfaces) reflects the degree of the bedform-crest-sinuosity, as well as the sub- to supra-critical angle at which the bedforms are climbing, which can then be classified as compound-dune (Allen, et al., 1982). Note that migration of isolated 3-D dunes can also generate a tangential cross-stratification with tabular lower and upper boundaries. Plant remains indicate a proximal position of the deposits within the system, while mud drapes testify to the impact of tidal processes

(Continues)

TABLE 1 (Continued)

Facies descriptions	
Facies	Description
F	Unidirectional-current ripple cross-stratified sandstone
	Very fine- to fine-grained dark- to light grey sandstone, displaying unidirectional-current ripple cross-stratification, climbing ripples occurring locally, commonly observed in upward thinning succession from Facies E. Bioturbation index (Taylor & Goldring, 1993) varies between 1 and 2
	VF-F
	Unidirectional-current ripples are the product of downstream migrating bedforms within unidirectional non-laminar flow conditions, representing for a given grain size, a lower energy level than the one generating Facies E or Facies H (Allen, et al., 1982). They can occur in a multitude of depositional environments (Allen, et al., 1982). Unidirectional-current ripples show the same maturity trend as they morph from straight-crested bedforms into 3-D ripples with the flow conditions (Venditti et al., 2005). Climbing ripples reflect a sedimentation rate exceeding the bedform progradation speed (Ashley, Southard, & Boothroyd, 1982) resulting in a positive aggradation
G	Oscillation ripple cross-stratified sandstone
	Very fine- to fine-grained dark- to light grey sandstone, dominated by oscillation ripple cross-stratification, characterized by a sharp to gradual lower boundary. Occasionally displaying false herringbone cross lamination. Sporadically displaying mud drapes, unidentified burrows and rare wood fragments, it occurs as isolated dm-thick beds, or in intervals up to 5 m in thickness, locally upward coarsening. Bioturbation index (Taylor & Goldring, 1993) varies between 1 and 2
	VF-F
	Oscillation ripples are a product of the waves propagation and are generally interpreted as upper shoreface deposits, although similar deposits have been documented in non-marine environments (Allen, et al., 1982, Basilici, 1997)
H	Plane parallel-stratified sandstone
	Very fine- to medium-grained dark- to light grey sandstone, featuring plane parallel-lamination (PPL) and plane parallel stratification (PPS), with a commonly sharp lower boundary, and occasional gradual transition from the underlying strata, scattered plant fragments, oscillation- and unidirectional-current ripples occurring sporadically Bioturbation index (Taylor & Goldring, 1993) varies between 1 and 2
	VF-M
	PPS is a characteristic sedimentary expression of burst-and-sweep traction flows undergoing laminar upper-flow regime conditions, although PPS can still form at lower flow intensities when the sediment concentration in the water column is high, and occur within a range of depositional environments (Cheel & Middleton 1993, PickeringStow, Watson, & Hiscott, 1986, Ashley, et al., 1990, Massari, 1996, Fielding, 2006). Plant fragments indicate a proximal location of the deposits within the system
I	Structureless sandstone
	Structureless very fine- to medium-grained, dark- to light grey sandstone
	VF-M
	The lack of stratification within a homogeneous sandstone can be linked to a very rapid deposition from suspended load or it can be due to an extremely high degree of bioturbation (Gingras, Pemberton, & Smith, 2015)
J	Heterolithic mud- to siltstone with lenticular bedding
	Very fine- to fine grained grey sandstone lenses within a laminated to undulating muddy to silty dark grey matrix, commonly found in upward coarsening intervals from Facies A into Facies J. The sandstone lenses are often characterized by uni- and bidirectional-current ripple cross-stratification. Bioturbation index (Taylor & Goldring, 1993) varies between 1 and 4
	Md-F
	Heterolithic deposits produced by a rapid flow deceleration and/or expansion within a mixed mud-sand-rich environment (Baas et al., 2016). Bidirectional-current ripples suggest a certain degree of tidal reworking. High bioturbation index indicate a well-oxygenated and life-prone sea-floor (Taylor & Goldring, 1993)

(Continues)

TABLE 1 (Continued)

Facies descriptions		
Facies	Description	Grain size Interpretation
K	Heterolithic silt- and sandstone with wavy bedding	Si-F Heterolithic deposits produced by a rapid flow deceleration and/or expansion within a mixed mud-sand-rich environment (Baas et al., 2016). Bidirectional-current ripples suggest a certain degree of tidal reworking. Rhythmic thickening and thinning interpreted as a response to cyclic waxing-waning tidal current over the area, such as neap-spring tidal cycles (Visser, 1980). High bioturbation index indicate a well-oxygenated and life-prone sea-floor (Taylor & Goldring, 1993)
L	Heterolithic sandstone with flaser bedding	VF-F Heterolithic deposits likely produced by waxing-waning tidal currents (Baas et al., 2016; Sato et al., 2011). Rhythmic thickening and thinning interpreted as a response to cyclic waxing-waning tidal current over the area, such as neap-spring tidal cycles (Visser, 1980). High bioturbation index indicate a well-oxygenated and life-prone sea-floor (Taylor & Goldring, 1993)
M	Coquina bed	Fl-RdSt In situ coquina beds are often found in high-energy environments, in which siliciclastics are washed out of the system and shell fragments display a bedding-parallel preferred orientation (Teyssen, 1984) or shell fragments can be transported and rapidly redeposited into a adjacent depocentre by storm-related events (ex situ coquina beds; Avila et al., 2015)
N	Paleosol	S-uVF In situ biogeochemically altered strata associated with paedogenesis and subaerial exposures (Kraus, 1999), potentially encapsulating a non-negligible period of time in comparison with other neighbouring facies (Bown & Kraus, 1993). The limited vertical connection between the different paleosols suggest non-steady sedimentation rates occurring at the time of deposition over the study area (Kraus, 1999)
O	Coal-rich horizon	Md-Si The genesis of coal and other coal-rich horizons require anoxic conditions within the shallow and sediments-starving column in order to preserve the organic matter, and often indicate swamp conditions; lacustrine coal also occurs (Miall, 2016)

In the western study area B and C, the photogrammetric model is used to subdivide the succession into three main sedimentary units. The first unit is delineated by the separation of faulted from non-faulted deposits with a thick sandstone interval marking the top (Figures 1b and 3). The second unit encompasses a very characteristic thick shale-rich succession capped by a sandstone interval. The final unit comprises the remaining exposures. This subdivision allows tentative correlation towards Øhmanfjellet, Tjuvfjordskarvet and the eastern study area, where a coarsening upward unit of similar thickness is overlain by a thick shale-rich interval of similar thickness to Unit 2. The units are labelled 1–3 and their bounding horizons are distinguished with colour coding (orange and green) throughout to simplify identification (Figure 1b–d). The logs at Schneiderberget and Næringstuva could not be directly correlated to the other logs or the photogrammetric model.

The observed lithofacies in the study area are detailed in Table 1. Distinct facies associations are defined in Table 2. Observations from the photogrammetric model are shown in Table 3. The succession is interpreted based on facies associations and observations from the model, and then further discussed with respect to the different units, covering variations across the study area and relationship to the regional infill of the Barents Shelf.

4.2 | Facies associations

4.2.1 | FA 1 offshore transition

FA 1.1 - Shelf and distal pro-delta slope deposits

Description. FA 1.1 is composed mainly of laminated mudstone with low sand content, grading upwards into sets of heterolithic mud- and siltstone, with scattered rippled sandstone lenses. These sediments are interbedded with deformed sandstone beds and lenses with dish-, flame- and loading structures (e.g. load casts, ball-and-pillow), convolute bedding and internal folding. Thin sandstone beds (ca. 2–20 cm) characterized by plane-parallel stratification (PPS) and asymmetric, unidirectional-current ripple cross-stratification occur either as individual layers or grading from PPS. Bioturbation, including *Taenidium* and *Helminthopsis*, commonly occurs with local intensity variation between 1 and 4 (after Taylor & Goldring, 1993), and increases as the succession coarsens upward into structureless sandstone.

Interpretation. The occasional planar parallel sandstone beds in FA 1.1 are river-driven hyperpycnites (Bhattacharya & MacEachern, 2009; Petter & Steel, 2006). The dominance of laminated mud- and siltstone, which settled from suspension, coupled with hyperpycnites and/or unidirectional-current ripple cross-stratified sandstone

beds, and the lack of oscillation-driven deposits indicate an offshore setting below the storm weather wave base (SWWB; Bhattacharya, 2006). This is supported by the variety of soft sediment deformation within some of the current rippled and PPS sandstone beds, interpreted as gravity-driven mass wasting deposits driven by floods and/or sediment failures (Bhattacharya, 2006; Bhattacharya & MacEachern, 2009; Moslow & Pemberton, 1988; Owen, 1987).

FA 1.2 – Wave-dominated lower delta front/offshore transition

Description. Facies association 1.2 is characterized by the occurrence of isolated, folded and deformed sandstone beds as well as hummocky (HCS) and swaley (SCS) cross-stratified beds in a heterolithic mud- and silt-dominated background with both lenticular- and wavy bedding. HCS is more common than SCS. A few centimetre thick sandstone beds with unidirectional-current ripples occur locally. Low-angle and tangential cross-stratified sandstone beds are increasingly abundant towards the top. FA 1.2 displays a characteristic upward-coarsening trend, as low-angle stratified sandstone beds become more abundant, thicker and more laterally extensive before grading into the overlying deposits of FA 2.

Interpretation. The occurrence of HCS and SCS places these deposits above the SWWB as a result of storm-induced oscillatory currents or instability events (Bhattacharya, 2006; Cheel & Leckie, 1993; Jelby, Grundvåg, Helland-Hansen, Olaussen, & Stemmerik, 2017; Quin, 2011), whereas the dominance of mud- and silt-dominated background sedimentation indicates a lower energy depositional environment still characterized by settling of suspended load. Mass wasting deposits and overall coarsening upward suggest a shallowing succession representing a prograding pro-deltaic environment subject to slope failures (Bhattacharya, 2006; Bhattacharya & MacEachern, 2009; Owen, 1987). Furthermore, unidirectional-current ripples in sandstone beds implies that FA 1.2 was deposited within a delta front setting (Jackson, Hampson, & Sech, 2009; Niedoroda, Swift, Hopkins, & Ma, 1984).

4.2.2 | FA 2 – Delta Front

FA 2.1 Tidally dominated delta front

Description. Gradually transitioning from the underlying FA 1, FA 2.1 features 10–20 m thick upward-coarsening packages from mud- to sandstone heterolithic deposits, with low-angle and tangential cross-stratified beds with interbedded unidirectional-current- and oscillation ripples. Cross-stratified sandstone strata are locally arranged in tidal bundles, or in rhythmic sand-mud couplets (Figure 7a,c)

TABLE 2 Facies associations of the studied succession

Facies association	Depositional environment	Key bedforms
FA 1		
FA 1.1	Offshore and distal prodelta slope	Laminated mud, event beds
FA 1.2	Wave-dominated lower delta front	Event beds, soft-sediment deformed sandstone, current ripples, HCS and SCS
FA 2		
FA 2.1	Tidally dominated delta front	Coarsening upward units, lower soft sediment deformation, tabular cross beds, bi-directional, TCS, tidal indicators
FA 2.2	Mouthbars	Coarsening upward heterolithic, inclined strata, plant material
FA 2.3	Storm-dominated delta front	HCS grading upward into TCS, wavy, PP sandstone. Overlain marine muds
FA 3		
FA 3.1	Subaqueous platform and tidal flats	Heterolithic sediments with lenticular-, wavy- and flaser-bedding, high bioturbation
FA 3.2	Tidal creeks/tidally dominated channels	Channel outer geometry, inclined heterolithic stratification, tabular cross-beds with subordinate current beds
FA 3.3	Wave-built sandbars	Coarsening upward low-angle cross strata, convex up CU or massive
FA 4		
FA 4.1	Delta plain with marine incursions	Paleosol, coal seams, washover beds
FA 4.2	Fluvial channels	Trough cross-stratified sandstones

and flaser bedding in fine-dominated heterolithic deposits (Figures 8d and 9h). Both oblique and sigmoidal cross-strata occur, and evidence of bi-directional currents is commonly observed as well as reactivation surfaces (Figure 8d,f). The base of these cross-stratified sandstone bedsets and lenses can be either erosive or sharp, and locally displays loading and convolute structures. Coal fragments together with mud-drapes and rip-up clasts occur along foresets within cross-stratified sandstone bedsets. The bioturbation index (Taylor & Goldring, 1993) varies between 1 and 3, and includes *Skolithos*. Laterally the deposits become thinner, displaying an overall coarsening upward trend and increased bioturbation and unidirectional-current indications. In the photogrammetric model, FA 2.1 forms laterally extensive bodies covering the entire outcrop (>9 km). Towards the

uppermost part the sandstones becomes erosive and well sorted with large-scale trough cross-stratification.

Interpretation. The upward-coarsening cross-stratified sandstones of FA 2.1 are interpreted to be a tidally dominated delta front associated with intense reworking of mouth-bar deposits. The strong tidal indicators which include sigmoidal cross-bedding, bi-directional cross-strata, reactivation surfaces, rhythmic lamination and bundling, compound cross-bedding, are all indicative of a shallow marine tidal environment (Allen & Honewood, 1984; Dalrymple, Knight, & Lambiase, 1978; Plint & Wadsworth, 2003; Rossi & Steel, 2016; Wei et al., 2016). Reworking favoured extensively amalgamated bodies compared to more isolated mouth bars (Rossi & Steel, 2016). The presence of symmetrical ripples indicates that the system was locally impacted by waves. An

TABLE 3 Sandbodies in the Kvalpynten photogrammetric model separated into the three units into which the section is subdivided

Sandbodies								
"Name"	Location	Grading	Width (m)	Height (m)	Features	Dip/Dip direction (average)	Heigh (from base unit)	Type
Unit one: growth-faulted lower cliff section, several distinct coarsening upward cycles separated by thick shales. Upper sandstone is continuous with flat top. 100–170 m thick succession exposed, basal boundary cliff top of Blanknuten Mbr.								
Inc 1	W-C	Rv	17+13	17	Coarsening up, shales and sands, 2D, 2 units	5.5°/221°		Mouthbar
Inc 2	W-C		17	17	Inclined heterolithic, capped by massive sandstone	2.4°/253°		Mouthbar
Inc 3	W-B		16	16	Incline heterolithic coarsening upward, capped by sandstone, unit progrades over faulting	4.9°/254°		Mouthbar
Unit two: averages 42 m thick. Two distinct sandstone bodies at the base and top, the lower consists of two coarsening upward intervals, the lower of which pinches out towards the south. The middle section is about 20 m thick, dominantly shaley with siltier intervals. The uppermost sandstone is a laterally continuous coarsening upward interval about 6–12 m thick. Characterized by much lateral continuity, no isolated sandbodies barring single channel and point bar.								
Channel 1	W-B	Nm	480	23	Appears asymmetric, southern edge has IHS point bar, erosive base		26	Tidal channel
Point Bar 1	W-B	Nm		11	Merges with CH 1	10°/11°		Point bar
Inc 4	W-B	Rv		9		6.1°/274°	30	
Unit Three: ca 200–225 m exposed. Shale marker base. Laterally continuous sandstone body ca. 8-m thick at base overlain by stacks of convex sandstone bodies with shale base and top. Middle section contains continuous sand and mud layers intersected by thick fining upward successions with prominent IHS at times eroding down significantly, uppermost sandstones are massive channel-shaped.								
Sandbody 1	W-C	Rv	600	12	Convex, possibly several layers	Flank 5°/28° (LA 8°/22°)	15	Sandbar/reworked mouth-bar
Sandbody 2	W-B	Rv	706	12	Convex, coarsening upwards, lateral accretion surface, mid-section of unit	Flanks 4°/260: 3°/31°	12	Sandbar/reworked mouth-bar
Sandbody 3	W-B	Rv	705	7	Convex, coarsening upwards, mid-section	Flanks 4°/60°: 5°/241° (LA 3°/59°?)	17	Sandbar/reworked mouth-bar
Sandbody 4	W-B	Massive	860	7	Convex, same level as sandbody 3, but clear pinchout (4 under 3)		18	Sandbar
Sandbody 5	W-B	Massive	750	6	Massive, sharp base and top, diffuse edges, same level as sandbody 3 and 4 but underlies southern tip of 4	Flank 3°/70°	20	Sandbar
Sandbody 6	W-C	Massive	175	6	Massive, convex, very distinct flank on one side	Flank 3°/35°	34	Sandbar

(Continues)

TABLE 3 (Continued)

Sandbodies								
"Name"	Location	Grading	Width (m)	Height (m)	Features	Dip/Dip direction (average)	Heigh (from base unit)	Type
Channel 2	W-B	Nm	3650 (tr)	32	Massive trough-x sandstone at base, in total up to 32 m thick, incised by 1500 m ca. 17 m muddy point bar lateral accretion NW	13°/301°	30	Tidal channel
Channel 3	W-B	IHS	1800	25	Erodes into underlying strata, very prominent IHS, Nm grading also variations in muddy-sandy intervals	12°/289°	29	Tidal channel
Channel 8	W-B	Nm	200	21	Appears massive trough x stratified fining slightly upward		27	Tidal channel
Channel 12	W-C	Nm	ca 330	7	Diffuse, vague lateral accretion ca 30°		34	Tidal channel
Channel 6	W-B	Nm	850	10	Very erosive base, sandstone appears quite massive trough cross-stratified, fining slightly upward		86	
Channel 7	W-B		510	7	Very erosive base, sandstone quite massive, hard to differentiate grading, appears symmetrical, thins towards both edges, same layer as channel 6		86	
Channel 4a	W-B	Nm IHS	1500	17	Cuts down into very dark mud on southern tip of Kvalpynten, more massive sandstone base fining up into IHS and muddy top	9°/17°	121	Tidal channel
Channel 4b	W-B	Nm IHS	2100	17	Fining up, in middle section two units with planar bed between. Clear inclined strata, muddy apparent towards north	11°/311°	119	Tidal channel
Channel 4c	W-B	Nm IHS	1200	12	Muddier interval shares level with 4a-b on separate cliff, sandy fining upwards into muddy inclined strata	19°/254°	117	Tidal channel
Point bar 2	W-B	IHS		15	Poorly resolved atop cliff, IHS very muddy, no basal sandstone	12,5°/300°	184	Point bar
Point bar 3	W-B	Nm IHS	100	7	Fining upward sand-rich, ends in muddy succession suggesting abandoned channel	10°/27°	192	Point bar
Channel 9	W-B		290	19	Appears relatively symmetric, internal structure not apparent, top of cliff		200	Fluvial distributary channel

(Continues)

TABLE 3 (Continued)

Sandbodies								
"Name"	Location	Grading	Width (m)	Height (m)	Features	Dip/Dip direction (average)	Heigh (from base unit)	Type
Channel 10	W-B		150	9	Laterally stacked beside channel 9, internal lateral stacks, asymmetric with one more prominent wing, top of cliff		204	Fluvial distributary channel
Channel 11	W-B		350	17	Appears relatively symmetric, internal structure not apparent, located at the top of cliff		195	Fluvial distributary channel

Note: Low-angle prograding.

Point bars.

Fluvial channel.

Tidally dominated channel (IHS).

Convex/lense shaped sandbodies. Each is given a name, to which it can be referred in text and other figures. The location corresponds to the subdivision in Figure 1. The colour-coordination corresponds to the sandbody classification type at the bottom of the table.

Abbreviations: IHS, Inclined heterolithic stratification; LA, Lateral Accretion; Nm, Normal grading; Rv, Reverse Grading; SB, Sandbody; Tr, Truncated (i.e. the full body is not exposed and the measurement corresponds to the present outcrop).

increased terrestrial and fresh water influence is corroborated by the rising sand-to-mud ratio in the system, the abundance of coal and plant fragments and low levels of ichnofabric diversity (Ahmed, Bhattacharya, Garza, & Li, 2014).

FA 2.2 Mouth bars

Description. FA 2.2 shares many traits with FA 2.1, but is less well sorted, contains larger amounts of organic material (Figure 3c,d) and is associated with more slumped beds (Figure 3f,h). The succession overall coarsens upward but includes metre thick fining upward tangential cross-stratified sandstones with rip-up clasts (Figure 3g) and reactivation surfaces (Figure 4). Grain-size is typically very fine to fine. Asymmetric ripples are prevalent in the lower successions whereas symmetric ones frequently occur up-section. Climbing ripples also occur. At Tjuvfjordskarvet, stacks of inclined strata indicate a dominant progradational direction (Figure 6h). Bioturbation is scarce and confined to single beds. Paleocurrent data from current ripples indicate an overall SW-directed influx at Vogelberget.

Interpretation. FA 2.2 represents unconfined mouth bars accumulating beyond the river mouth. The high degree of organic material, soft sediment deformation, climbing ripples and current ripples and poorly sorted heterolithic accumulations are associated with strong river influence (Olariu & Bhattacharya, 2006; Olariu, Steel, & Petter, 2010; Rossi & Steel, 2016; Tye & Coleman, 1989). A sharp base with local loading structures, an absence of subaerial exposure indicators (e.g. mottling, paleosols), low-angle cross-stratification and dominantly laterally accreting sand bodies are some of the diagnostic features of rapidly accreting mouth-bar deposits (Ahmed et al., 2014; Martini & Sandrelli, 2015; Schomacker, Kjemperud, Nystuen, & Jahren, 2010). The heterolithic nature and occasional minor reworking of sedimentary material, wave-ripples and flaser bedding reflect variations in discharge. The fining upward packages within the succession represent minor distributary channels forming atop the mouth bars during periods of high discharge.

FA 2.3 – Storm-dominated delta front

Description. FA 2.3 consists of 6–8 m thick, sharp-based evenly thick or coarsening upward sandstone packages. They commonly include HCS and grade into undular, wavy or low-angle cross-stratification towards the top, with plane-parallel tops in places (Figure 5). The tops of these units are capped by mudstones. Organic material appears absent and bioturbation is often moderate but ranges from 1 to 4. FA 2.3 develops in the east study area, stratigraphically equivalent to the transition from FA 1 to FA 3 in the west study area where FA 2.1 dominates.

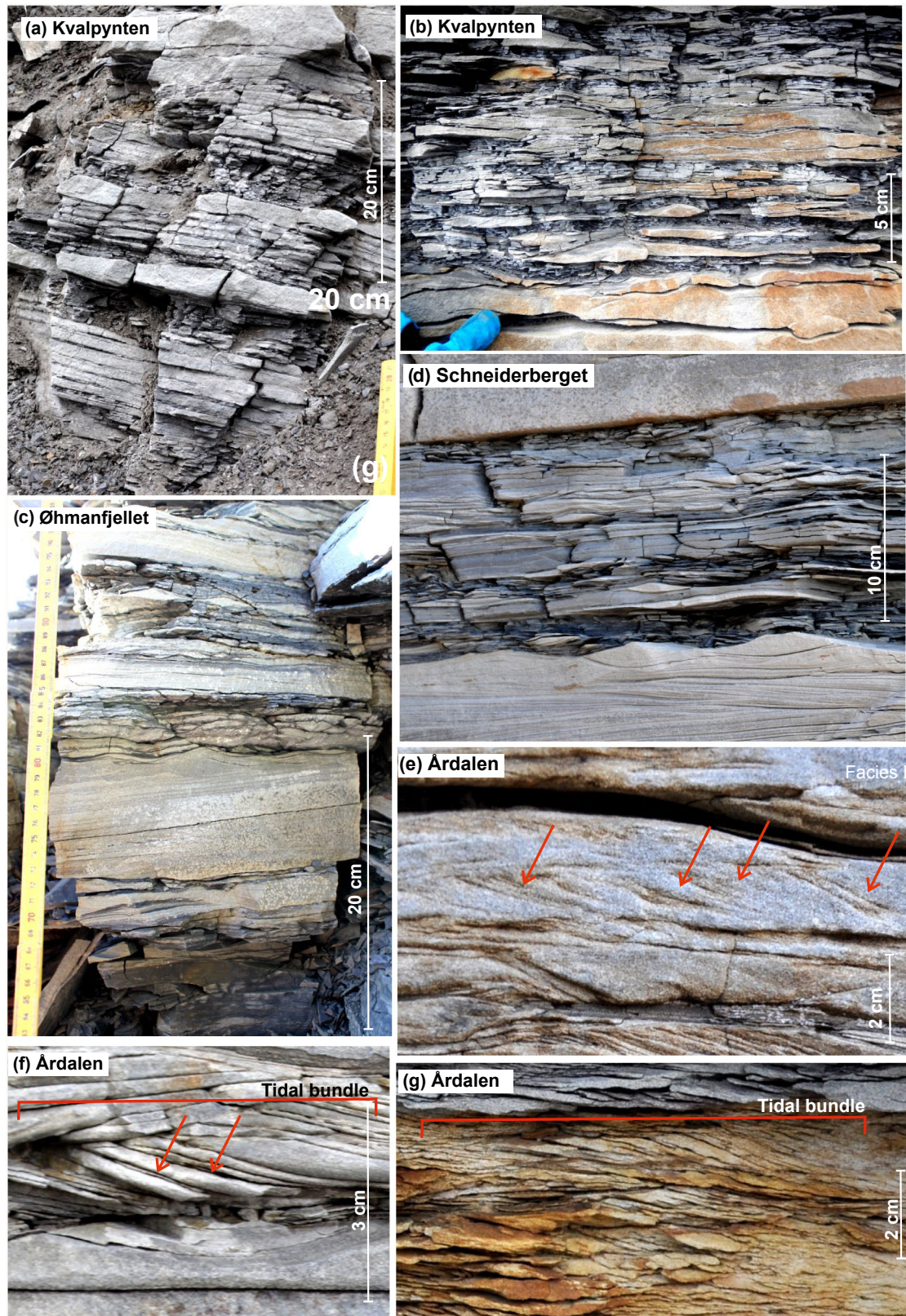


FIGURE 7 Examples of tidally dominated deposits from different locations in the study area. (a) Rhythmically stratified heterolithics, from Kvalpynten W, Unit 1. (b) Beds of flaser-wavy-lenticular heterolithics, from Kvalpynten W, Unit 1. (c) Heterolithic tidal deposits showing rhythmic stratification, Øhmanfjellet, Unit 1. (d) Hummocky storm beds overlain by wave-surfaces and heterolithic tidal flat deposits, Schneiderberget, Unit 2 (e) Double mud-draperes, marked with arrows, in a fining upward rippled laminated rock, Årdalen, Unit 3. (f) Double mud-draperes in a tidal bundle, Årdalen, Unit 3. (g) Tidal bundle in a ripple-laminated rock which also displays climbing ripples, Årdalen, Unit 3

Interpretation. The dominance of HCS indicates deposition below fair weather wave base where oscillatory flow, associated with storms, is the most common hydrodynamic

mechanism (Cheel and Leckie, 1993; Dumas & Arnott, 2006; Peters & Loss, 2012). The planar lamination is associated with upper flow regime during intense wave action. The close

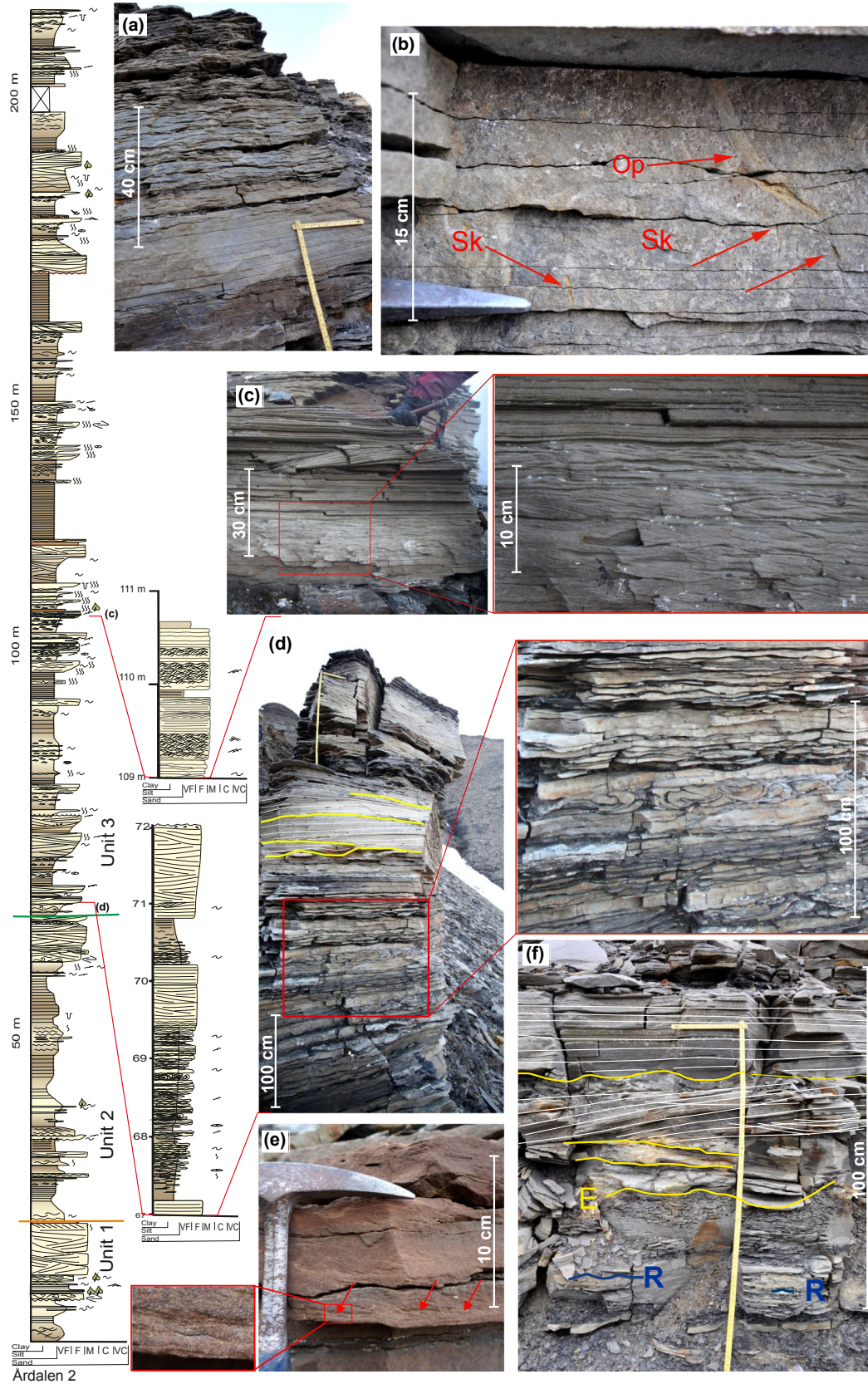


FIGURE 8 Showing the log from Årdalen 2 with some smaller logs showing the detail to which the area was logged originally. The photos show examples of the deposits encountered in the Årdalen area. (a) A fining upward succession interpreted as tidally dominated channel fill (FA 3.2) from Årdalen 1 log, ca 30 m up in Unit 3 (b) Trace fossils *Ophiomorpha* and *Skolithos* about 45 m up into Unit 3 at Årdalen 1 log. (c) Ripple rock coarsening up into planar parallel strata see closer details in box, located ca. 50 m up in Unit 3 at Årdalen 2 log, shown on log to the left. (d) Heterolithics in a tidal dune (FA 2.1), note small-scale convoluted successions (details to the right) and cross-strata with reactivation in the coarser uppermost succession. (e) Lower medium red coloured ripple-rock showing dominant direction of influx and organic-rich laminae on toe-sets marked with red arrows and seen better on the small enlargement to the left, ca. 10 m up into Unit 3 at the Årdalen 1 log. (f) Low-angle cross-strata and reactivation surfaces (marked with E, for erosion) in a subaqueous tidal dune with an erosive base, from Årdalen 1 log, ca. 40 m up into Unit 2 showing renewed progradation following the maximum flooding surface (MFS). In the heterolithics underlying the main sandbody wave-ripples are apparent marked by R

association with tidally reworked deposits of FA 2.1 suggests FA 2.3 was also modulated by tides. The overall observed higher degree of bioturbation suggests a lower energy setting compared to the west. FA 2.3 is therefore interpreted to represent a storm-wave-dominated, tidally modulated delta front.

4.2.3 | FA 3 Subaqueous platform

FA 3.1 Subtidal flats

Description. FA 3.1 dominates the upper part of each measured section and is closely associated with FA 3.2, grading upwards in FA 4 (Figure 4). FA 3.1 comprises a range of sedimentary features but is dominated by heterolithic, lenticular, wavy and flaser bedding (Figure 7b,d). Asymmetrical ripples commonly feature double mud-drapes and tidal bundling (Figure 7e–g). Minor sandstone bodies are massive and show erosive bases, or coarsen upward, commonly featuring wave and current ripples, cross-strata, both as individual decimetre-scale cross-sets and smaller centimetre-scale compound cross-sets (Figure 8c–f). Other notable features include the presence of complex bi-directionality in ripple-laminated beds in places giving rise to false herringbone structures (Figure 9a), plane-parallel laminated sandstones, short wave-length HCS (Figure 9c,e) and shell gravel. The bioturbation index (Taylor & Goldring, 1993) ranges between 1 and 5 and is commonly intense, completely obliterating original features. Recognized burrows notably include *Skolithos* and occasional *Ophiomorpha* (Figure 8b). FA 3.1 is differentiated from FA 4.1 by lacking continental indicators such as coal intervals or paleosols.

Interpretation. The intensity of identified bioturbation indicates a marine environment and, given the strength of tidal indicators, dominated by tidal processes. The presence of lenticular and wavy bedding and extensive bioturbation indicates a relatively lower energy in comparison with the delta front. The subaqueous portion of a compound clinof orm system (Kuehl, Levy, Moore, & Allison, 1997; Patruno et al., 2015; Pirmez et al., 1998; Roberts & Sydow, 2003; Swenson, Paola, Pratson, Voller, & Murray, 2005) is the

relatively flat and shallow area between the lower delta plain and the rollover of the delta front. The wealth of tidal indicators grading into the delta plain deposits indicates that this FA represents tidal flats (Baas, Best, & Peakall, 2016; Sato, Taniguchi, Takagawa, & Masuda, 2011). Sand-flats are characterized by current and wave-rippled, cross-laminated very fine and fine-grained sandstone, with common mud-drapes (Desjardins, Buatois, & Mangano, 2012). Mud-drapes along foresets of 3D migrating dunes also indicates a bimodal flow velocity system, characteristic of tidal currents (Visser, 1980). Unidirectional-current rippled beds commonly display loading and water-escape structures which imply a rapid deposition from overbank spills. Hence, they are directly linked to the proximity to distributary channels, with which they interfinger, testifying that these tidal flats developed in interdistributary areas (Elliott, 1974, Kurcinka, Dalrymple, & Gugliotta, 2018). Tidal flats commonly display a high degree of bioturbation (Desjardins, Buatois, & Mangano, 2012; Fan, 2011; Hughes, 2012; Mángano & Buatois, 2008). The appreciable wave influence is suggested by the presence of wave-ripples, short wave-length HCS (Figure 9c,e) and shell gravel indicative of storm events (Figure 9d,g) acting in open coast tidal flats. Such environments have been described from several locations around the world and represent an intermediate member between tidal and wave-dominated systems (Fan, 2011; Yang, Dalrymple, & Chun, 2005). However, unlike Edgeøya, open coast tidal flats often predominantly preserve wave-dominated successions which are only subtly different from true shorefaces, consequently open coast tidal flats might easily be misinterpreted in the rock record, and typically display strong seasonality (Yang et al., 2005).

FA 3.2 Tidal creeks and tidally dominated channels

Description. FA 3.2 consists of 5–10-m thick sandstone bodies with a lower erosive concave to flat boundary. The sandbodies occur in Unit 3 and are characterized by a fining upward trend and typically consist of multiple tabular layers around 5–20 cm thick with dominant cross-bed direction and sub-parallel beds in between (Figure 5). They can also be characterized by tangential cross-strata, fining upward into heterolithic deposits, often with symmetrical ripples as seen

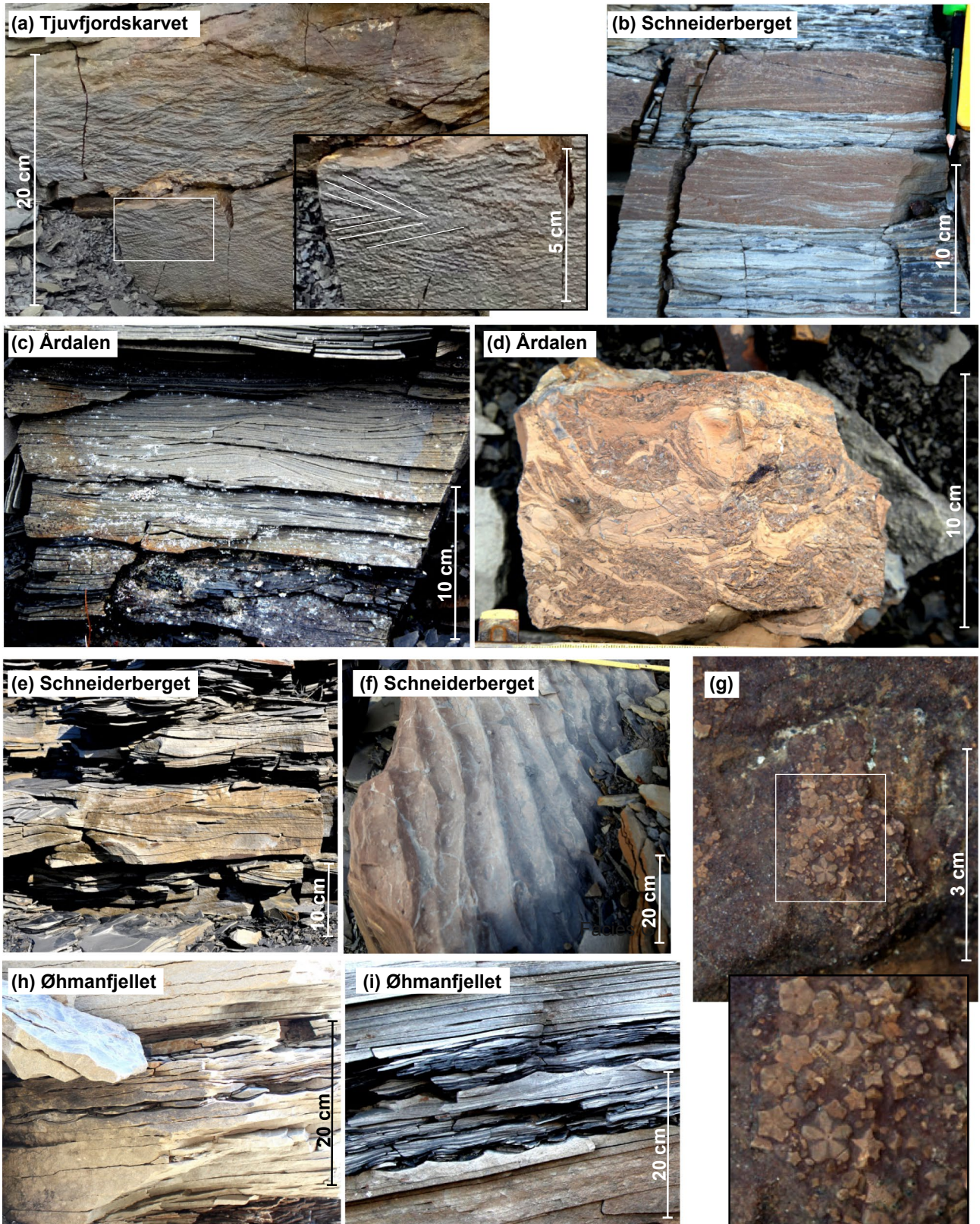


FIGURE 9 Examples of wave-dominated deposits. (a) False herringbone in wave-rippled (Facies G) rock from Tjuvfjordskarvet. (b) Heterolithics interbedded with red coloured wave-deposited beds, the lower an oscillation rippled rock (Facies G) with eroded ripple crests and the upper a low-angle cross-stratified sandstone (Facies D) from Schneiderberget. (c) Small-scale hummocky cross-strata from Årdalen Unit 3. (d) A storm-deposited shell-bed from Årdalen, Unit 3 (ca. 180 m up on log). (e) Small-scale hummocky cross-beds from Schneiderberget, Unit 3. (f) Wave-rippled surface from Schneiderberget, Unit 3. (g) Small crinoid fragments in a storm bed. (h) Wave-rippled surface underlying lenticular bed, Øhmanfjellet, Unit 1. (i) Heterolithic strata in a subaqueous dune including wave-rippled surfaces from Øhmanfjellet, Unit 1 (Photos a, g, h courtesy of Tore Klausen)

in the west study area (Figures 3a and 4). The sandbodies typically display very limited bioturbation in the lowermost parts (BI 0–1). Asymmetrical ripples are common, particularly in their upper parts, where the BI ranges from 1 to 3. Plant and wood fragments commonly occur throughout FA 3.2. On the photogrammetric model inferred depositional equivalents to FA 3.2 are observed in the form of inclined heterolithic stratification (IHS; Figure 6g). Two such bodies about 30 m up into Unit 3 are both ca 1,500 m long, 25 and 17 m thick respectively with IHS dipping 8–14 degrees west-northwest (Table 3 – Channel 2,3; Figure 6f,g). Another succession of IHS is observed ca 120 m up in Unit 3 which has a basal sandstone body exposed along almost the whole cliff-face (ca. 6 km), but it is dissected by present day valleys and thus measured as three units (Channel 4 a-c, Table 3, Figure 6b,c). The packages are ca. 15-m thick, fining upward from massive and trough cross-stratified sandstone into inclined heterolithic strata dipping 8–13° west, northwest and north respectively, northward along the cliff-face (Table 3). The channel cuts down into very black mudstone on the southernmost point of Kvalpynten.

Interpretation. The erosive lower contact and tidal and minor wave reworking, of these multi-story sand-bodies indicate a channelized environment within a marginal marine system (Ahmed et al., 2014; Olariu & Bhattacharya, 2006). The presence of tidal indicators, as well as the abundance of unidirectional-current ripples suggest a mixed zone of tidal and fluvial influence in the lowermost encountered channels (Olariu & Bhattacharya, 2006) which is supported by the low levels of ichnofabric diversity and limited degree of bioturbation. The presence of plant material, occasionally as coalified wood fragments, suggests many of these channels were connected to fluvial distributary channels.

On the photogrammetric model the tidal channels are observed as large-scale IHS (Figure 6), which attests to a highly meandering network of channels, at times reworking almost the whole area. Tidal point bars are commonly characterized by inclined heterolithic stratification resulting from changes in hydrodynamic regime characteristic of tidal settings (Dalrymple & Choi, 2007; Hughes, 2012). Since the tidal prism increases seaward, tidal channels also increase in width (Dalrymple & Choi, 2007). The wider channels with higher discharge curve less so the sharper meanders are typically found closer to the shore and represent the site of lowest hydraulic energy between the fluvially and tidally dominated parts. Tidal channels thus tend to coalesce into massive deep straight channels in the distal delta front, which individually reach widths up to several kilometres (Cummings, Dalrymple, Choi, & Jin, 2015). Similarly, tidal channels and creeks, which dissect tidal flats, are usually small to medium in the muddy, upper inter-tidal zone, forming deeper and wider channels in the lower sandy areas (Dalrymple, 2010).

All the successions of IHS share comparable dimensions and direction, with meanders migrating more or less north. The upper IHS, however, has a basal cross-stratified unit likely representing a channel lag unlike the two lower units, which display only the inclined strata. This suggests that the upper unit formed in the proximal part of the fluvial-tidal transition as the coarse-grained fluvial input decreases seaward (Dalrymple & Choi, 2007). Two thick sandstone bodies about 100 m above the Unit 1 - Unit 2 transition found at Grindane 1 and Årdalsnuten 2 (Figure 4), are characterized by sharp-based bedsets in heterolithic FA 3.1 These comprise thick or stacked trough cross stratified bodies with rip-up clasts, current ripples and minor organic material. They do not share many traits with FA 3.2 but are interpreted to represent basal deposits of subaqueous tidal channels similar to that observed in the photogrammetric model.

FA 3.3 - Wave-built sand-bars

Description. FA 3.3 consists of coarsening upward intervals up to 10 m thick with metre-sized low-angle cross-stratified, occasionally trough cross-stratified sandstones towards the top (Figures 4 and 5). FA 3.3 commonly occurs at the interface between FA 2.2 and the overlying deposits of FA 3.1, becoming progressively scarcer up-section where coarsening upward bodies are generally thoroughly bioturbated and sandstone beds thinner. Tidal indicators are rare, although occasional mud-drapes and double mud-drapes are found in the more heterolithic lower parts. Current indicators are common but the tops are often marked by wave-ripple surfaces, red coloured layers with occasional organic drapes (Figure 8e) and, in one instance, a conglomeratic lag (Figure 5). Bioturbation is often moderate. On Kvalpynten FA 3.3 occurs within the same horizon as a number of sand-lenses seen in the photogrammetric model (Table 3, Figure 6d,e). These lenses are convex up, massive or coarsening upward, 6–12 m thick and around 700 m long. The flanks of the sand-bodies dip around 3–5° southwest and northeast respectively. Internal surfaces observed in one body show accretion towards the northeast. The logged intervals and convex bodies in the photogrammetric models are of similar thickness and occur over the same narrow interval in Unit 3. They are therefore assumed to represent the same feature and the interpretation is based on combining observations from log and model.

Interpretation. Multiple interpretations for these features can be considered. The coarsening upward trend, wave-indicators and bioturbation establish a marine setting and the observed association, being located at the interface between FA 2 and FA 4, suggests that these sand-bodies formed atop the subaqueous platform in a largely unconfined setting. The occurrence of traction-flow related bedforms, as well as the dominance of fair weather oscillatory flow

over unidirectional- and storm-related oscillatory currents places these deposits within an upper shoreface depositional setting (Jackson et al., 2009; Moslow & Pemberton, 1988; Niedoroda et al., 1984). The occurrence of the FA at the offshore to delta plain transition suggests a very proximal near-shore location. The lack of soft sediment deformation, climbing ripples and plane-parallel deposits (Rossi & Steel, 2016) commonly related to mouth bars, suggests they are likely wave-built features. Persistent low-angle cross stratification within the units suggest wave action was the dominant mobilization agent prior to sediment storage. The sand-bodies dominantly display internal north-eastward accretion as well as overlap of bodies on northern flanks of other bodies, suggesting that the units accreted northward, away from the general westward (even south-westward) infill of the delta front. They could therefore have developed in a way similar to ancient berms composed of swash-overwash deposits characterized by mostly landward accreting low-angle cross-beds (Otvos, 2000), or as inter-tidal swash bars developed at the terminus of longshore transport systems (Hine, 1979). Atop the subaqueous platform of the tidally dominated Han River, swash bars are common features (Cummings et al., 2015). Subtidal shoals are another possible candidate given their convex up geometries (McIlroy, Flint, Howell, & Timms, 2008). FA 3.3 are thus under some debate but are interpreted to represent wave-built sand-bars.

4.2.4 | FA 4 Delta Plain

FA 4.1 Delta plain with frequent marine incursions

Description. FA 4.1 is characterized by a heterolithic assemblage of laminated mudstone and isolated sandstone beds with tangential cross-stratification and unidirectional-current ripples (Figures 4 and 5). The difference between FA 4.1 and the underlying FA 3.1 deposits is a scarcity of tidal indicators and the occurrence of coquina beds (rudstone) displaying chaotic bedding, paleosols and thin (5–20 cm) coal seams (Figure 10f–h,p). Reddish, well cemented carbonate layers with development of cone-in-cone structures occur at several locations (Figure 10c–e). Sandstones are generally thin, organic material prevalent and oscillation ripples are common. Bioturbation generally decreases compared to FA 3.1 but is locally intense (Figure 10b,n). Preserved sedimentary structures include low-angle cross-strata to distorted sub-parallel and tabular cross-laminated unidirectional-current rippled rocks.

Interpretation. FA 4.1 is interpreted to represent a lower delta plain succession. The presence of coal seams and paleosols in the succession indicates a continental setting on which anoxic marshes developed (Bown & Kraus, 1993; Kraus, 1999; Miall, 2016). The interbedded occurrence

of chaotically arranged *ex situ* coquina beds testifies of episodic storm events transporting shell fragments from the coast (Ávila et al., 2015; Teyssen, 1984). Marine incursions as well as overbank spills are expressed as tangential- and unidirectional-current ripples in cross-stratified sandstone beds and wave-ripples (Shen et al., 2015). The very thin coal seams (5–20 cm) and repetitive marine incursions suggest an extensive delta plain which was regularly flooded.

FA 4.2 Fluvial channels

Description. FA 4.2 is characterized by medium-grained sandstone bodies with erosive sharp bases with a subtle upward-fining trend (Figure 10a). The main sedimentary structures are large-scale (ca. 0.5–1 m), trough cross-stratification with organic drapes on the toes of cross-strata (Figure 10i). No bioturbation is observed. From the photogrammetric model, these isolated bodies are 150–350 m wide and 9–17 m thick (Figures 6b and 10k) and generally show limited lateral accretion or point bar development. The largest measures 350 m wide and 17 m deep, the smallest one measures 150 m wide and 9 m deep and has developed as a lateral offset stack. The medium to coarse sandstones form the coarsest deposits encountered in the study area. They occur exclusively up-section in Unit 3 and are always associated with FA 3.1–4.1. Two upward-fining inclined successions occur just below the massive sand-bodies. The upward-fining successions consist of laterally accreting beds 6–12 m thick, poorly resolved but dipping around 5–10 degrees in an overall north-northwest direction.

Interpretation. FA 4.2 are fluvial channels given the lack of marine influence or reworking, along with predominance of terrestrial material and the close association with FA 4.1. The up-section scarcity of tide-related bedforms advocates for a prograding coastline accompanied by dominance of fluvial processes with time (Kurcinka et al., 2018). The northward-accreting point bars observed below the fluvial channels indicate a continued westward-directed influx.

4.3 | Interpretation of stratigraphic units

4.3.1 | Unit 1

Unit 1 forms a stacked progradational delta-front succession comprising the shales of the Tschermakfjellet Formation and the lowermost sandstones of the De Geerdalen Formation, which form coarsening upward (CU) units (Smyrak-Sikora et al., 2019). The base of the unit is delineated by the top of the Blanknuten Member, where visible (Figure 3), or else by the present sea level, and the top by a continuous cliff-forming sandstone (orange marker, Figure 1) which drapes the

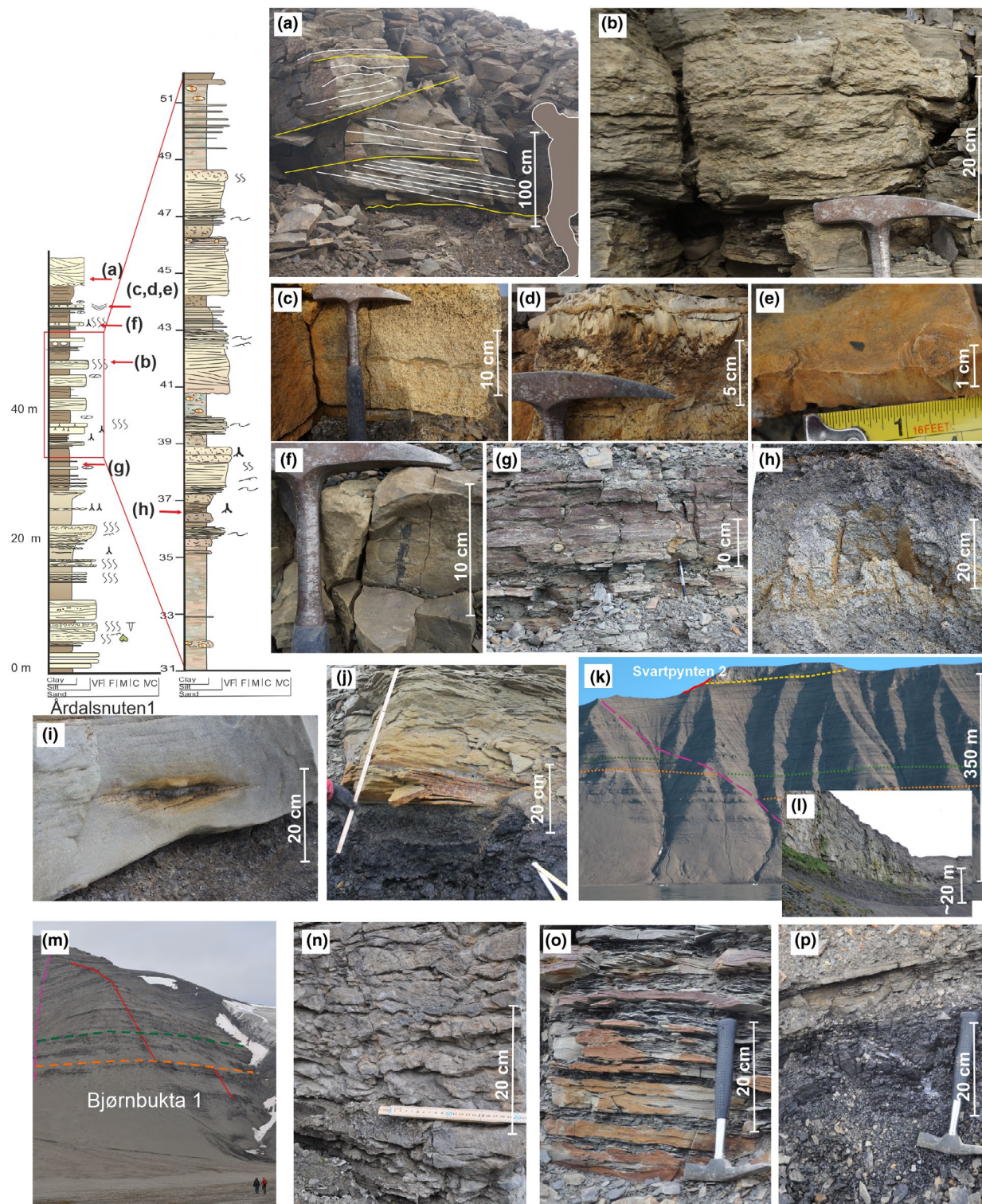


FIGURE 10 Årdalsnuten 1 log with a more detailed section including colour. Examples from photos are shown displaying (a) trough cross-bedding in a channel and (b) thoroughly bioturbated sandstones typical of the tidal flats. (c), (d) and (e) show the orange mottled appearance of the cemented layer displaying cone-in-cone development. (f) Example of a root (g) mottled coloured layer with concretions (h) Paleosol. Below the Svartpynten 2 log (k) with the massive channel body at the top of the mountain as shown in the photo and in (l). (j) Shows organic material at the base of cross-beds and (h) organic-rich bed with sand-layer incising. (m) A photo showing the location and extent of the Bjørnbukta 1 log and examples of deposits from this location with (n) showing cryptobioturbated deposits and (o) displaying heterolithic deposits featuring lenticular bedding and (p) showing a thin coal seam

faulted succession. Around Kvalpynten 100–135 m of vertical thickness is exposed and towards Vogelberget, where the Blanknuten Member outcrops, the full unit thickness of ca. 175 m is exposed (Figure 3). The lowermost section of the unit is characteristic of pro-deltaic deposits (FA 1.1) in an unrestricted, open marine environment, given the amount of mud, bivalve fragments and a full marine trace-fossil suite. Occasional gravity-driven event beds and storm beds represent the main delivery of sand (Figures 4 and 5).

The delta front is represented by three to five stacked upward-coarsening units (CUs), 25–60 m thick (Smyrak-Sikora et al., 2019; Figure 6). Characteristic for the CUs within the fault blocks in the western part of the study area is a strong tidal influence (FA 2.1) in the form of double mud-drapes, tidal bundling of strata and decimetre thick heterolithic lamination showing sand-mud couplets, reflecting neap-spring tidal cycles (Figures 5 and 7). Although not unequivocal tidal signatures, the wealth of indicators and occurrence of all three types support a dominance of tidal influence on the deposits (Dalrymple, 2010; Davis, 2010; Nio & Yang, 1991; Wei et al., 2016). The delta front is interpreted to have consisted of a laterally extensive and amalgamated compound dune field. The heterolithic deposits grade upward into coarser, cleaner compound trough cross-stratified sandstones with mud-chips and reactivation surfaces which, given the lack of terrestrial influx and often gradual transition, likely comprise smaller amalgamated 3D dunes. The smaller size and cleaner sands are interpreted to reflect increased tidal energy conditions and higher degree of reworking resulting from vertical restriction as accommodation was filled (Cummings, Arnott, & Hart, 2006).

Growth-faulting significantly controlled variations in accommodation in the succession likely favoured by rapid loading atop pro-delta muds (Ogata et al., 2018; Smyrak-Sikora et al., 2019). Deposition was then focused in the accommodation created, which trapped significant mudstone accumulations between isolated sandstones compared to more continuous deposition in un-faulted deposits nearshore (Figure 6). The unit merges into a more uniformly heterolithic succession at Vogelberget where CUs are more discrete (Figures 3,4). The area around Vogelberget coincides with an increased fluvial influence and development of more characteristic mouth-bar deposits (FA 2.2). The fluvially dominated mouth bars form stacked CUs commonly displaying gently inclined heterolithic strata dipping 2–5° south-westward (Table 3, Figures 3d,6h). The base of the inclined strata appears undular and slightly erosive, cutting into muddy heterolithics in places, creating an angular unconformity between underlying and overlying beds. The uppermost CU is generally capped by an erosive, clean trough cross-stratified sandstone interval, the base of which could mark a maximum regressive surface. Mud-rich deposits dominate east of Vogelberget at Øhmanfjellet (Figure 3), and tidally reworked sandstones are

akin to isolated dunes (Olariu, Steel, Dalrymple, & Gingras, 2012) indicating a dominantly interdistributary area. Towards the eastern study area the delta-front deposits show a higher degree of storm influence (FA 2.3, Figure 5).

The joint occurrence of mouth bars, storm-dominated and extensive tidally dominated deposits, reflects a delta front with spatially and temporally variable sediment input. Parts of the delta system were not redistributed by tides, possibly during periods of high sedimentary discharge. The mouth bars are poorly sorted and mud-rich compared to the redistributed sediment, which was reworked into better sorted, laterally amalgamated sandstones. Unit 1 shows a strong wave-dominance in the delta front (FA 2.3) toward east (Figure 5). This difference is interpreted to reflect lower sedimentation rates in the east, favouring winnowing and washing over by storms. Lower sedimentation could also result in a narrower platform and thus less dampening of the waves, further enhancing their impact on the deposits (Choi, Dalrymple, Chun, & Kim, 2004; Cummings et al., 2015; Feldman & Demko, 2015).

4.3.2 | Unit 2

The dominance of shelf and distal pro-delta slope deposits in Unit 2 indicates a deepening relative to underlying deposits, and is interpreted to represent a transgressional interval with a maximum flooding surface placed within the thickest shale interval (Figures 4,5). The characteristic interval is applied as a regionally traceable marker (Anell, Faleide, et al., 2016; Anell, Lecomte, et al., 2016; Osmundsen et al., 2014). The lowermost sandstones form retrograding parasequence stacks which become thinner and finer up-section, preceding a ca. 10 m thick, almost completely shaley interval, occurring prior to renewed progradation. The unit is 37–48 m thick around Kvalpynten. It generally consists of one or two basal coarsening upward successions totalling ca. 10 m. In the north part of western Kvalpynten this lowermost part is relatively sand-rich, with the basal interval consisting of two coarsening upward cycles, each 4 m thick (Figure 6f). The lowermost of these sandstones pinches out towards the south, indicating continued southwest directed influx, as indicated by the dip of the underlying mouth bars (Table 3).

Renewed progradation mirrors the respective underlying deposits with a tidal compound dune field (FA 2.1) in the west and a storm-dominated delta front (FA 2.3) toward the east. However, the strong storm influence in the eastern study area is replaced by a stronger tidal signal in the lowermost transgressive beds (Figure 5), testifying tidal amplification during transgression (Boyd, Dalrymple, & Zaitlin, 1992; Dalrymple, 2011). The lack of well-developed 2D dunes in the west suggests that accommodation remained limited, favouring compound 3D dunes characterized by clean,

erosive-based and reworked sandstones. A single subaqueous channel is preserved in Kvalpynten where a fining upward IHS succession dipping 10 degrees northward merges with a massive down-cutting sandstone unit, 480 m long and 23 m thick (Table 2, Figure 6f). The northward propagation of the point bars suggests that the sedimentary influx following transgression was directed more westward, in line with the paleocurrents measured in the uppermost units (Figure 11).

4.3.3 | Unit 3

Unit 3 covers the uppermost part of the section and is variably exposed across the study area with a thickness of ca. 100–200 m. At Vogelberget Unit 3 is entirely eroded and reappears at Øhmanfjellet. A shale interval atop the uppermost sandstone in Unit 2 marks the base (Figures 1,6).

Unit 3 is interpreted to record the highstand passage of the delta front (FA 2) across the subtidal flat (FA 3) and onto the delta plain (FA 4; Figures 4,5,12,13). It forms an overall progradational package, characterized by the upward increase and thickness of delta plain deposits as typified by the log at Naeringstuva (Figure 5). A highly aggradational component is reflected in the stacked parasequences and the high occurrence of oscillation ripples in sandstones interbedded

between root-casts and coal seams (Figure 10f,h,j,p), together with the typical organic-rich overbank deposits. The rapid changes between a subaerial peat mire and shallow subtidal environments reflect a widespread lower delta plain aggradation, with frequent marine incursions. A similar development is seen in the De Geerdalen Formation on Hopen (Klausen & Mørk, 2014) and in the tidally influenced Jurassic deposits offshore Norway (van Cappelle, Ravnås, Hampson, & Johnson, 2017).

In Unit 3, previous laterally homogenous deposits are replaced, along- and up-section, by a range of different types of sandstone bodies. This Unit marks the transition from the delta front to the delta plain settings through a subtidal flat (FA 3.1). The subtidal flat was dissected by tidal creeks and tidally dominated channels (FA 3.2), and occasionally isolated wave-build sand-bodies developed atop the flat (FA 3.3; Figure 12). This subtidal flat is typified by highly bioturbated, commonly cryptobioturbated, heterolithic tidal deposits. Sandy flats are typically intensely bioturbated due to the high infaunal biomass, low-energy, limited subaerial exposure and low sedimentation rates (Dashtgard, 2011; Desjardins et al., 2012; Fan, 2011; Gingras, Pemberton, Saunders, & Clifton, 1999). These sites are commonly located at some distance from the river mouths, where brackish water and high sedimentation rates result in low bioturbation

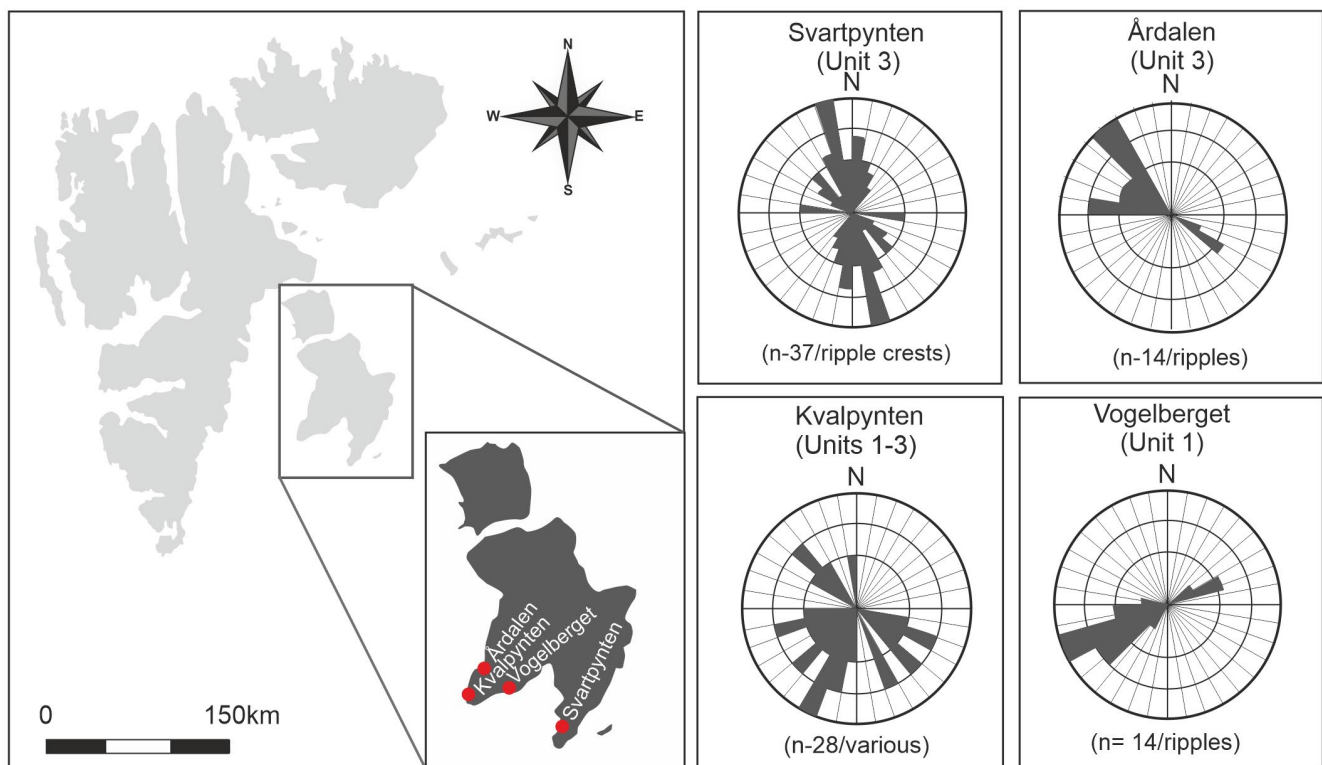


FIGURE 11 Paleocurrent measurements from four areas on Edgeøya. Note that the measurements from Svartpynten record ripple crests and thus the displayed results are bimodal and represent the orientation of the coastline. The display accentuates the dominance of a SW-directed inflow for Unit 1 (Vogelberget), towards a more W-NW directed inflow in Unit 3, which is corroborated by the photogrammetric analysis

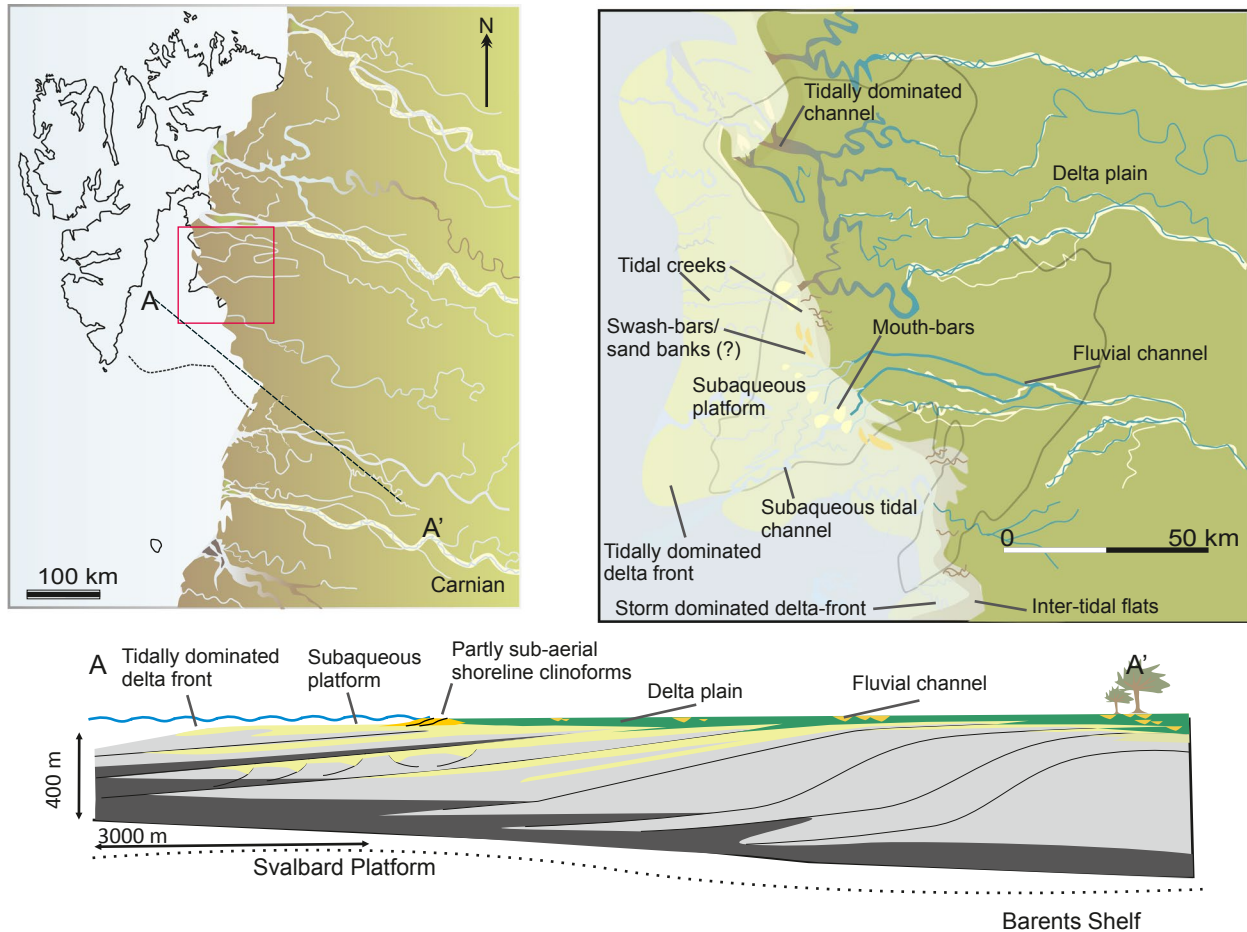


FIGURE 12 A depositional model for the formation of the De Geerdalen deposits on Edgeøya around the Carnian time period featuring a large prograding delta plain advancing NW and increasingly W across the Barents Shelf. The close-up shows a cartoon of the inferred depositional system with a tidally dominated compound dune field making up the delta front which is de-coupled from the coastline separated by an extensive subaqueous platform dissected by tidal channels. Mouth bars develop near the coast and further from the main influx the platform is narrower and becomes storm-dominated. The 2D cartoon cross-section A-A' at the base shows a simple schematic of an advancing clinoform succession with large prism-scale clinoforms becoming less steep and less high across the Svalbard Platform and tidal amplification moving more sand greater distances from the shoreline

(MacEachern & Bann, 2008). Alternatively, the high intensity of bioturbation observed in many sandstones could also attest to low sedimentation rates in a channelized environment with stable salinities, and may record the infill of abandoned tidal channels and creeks (Legler et al., 2014), given the association with FA 3.2.

The thick fining upward IHS intervals at several levels are interpreted as point bars of tidal channels, or, if directly connected to the fluvial system, tidally dominated channels given their likeness to studied tidal channels elsewhere (Figure 12). The scale of the IHS at Kvalpynten (25 m thick/ 8–15° dip and 15 m thick/12.5° dip) indicates very large channels, similar in dimensions to those of the Han River Delta (15–40 m deep), where IHS of near identical dimensions have been observed (25 m dipping 14°; Choi et al., 2004; Cummings et al., 2015). The size at Kvalpynten also matches those of the Aptian McMurray Formation in Alberta Canada (25 m/8–12°; Martinius et al., 2017) and

the Mid-Cenomanian Dunvegan Formation in the western Canada Foreland Basin (15 m; Plint & Wadsworth, 2003). The dimensions of the channels indicate they all formed in the subtidal zone. The extensive lateral accretion attests to a highly sinuous network of channels. The two IHS intervals around 30 m up in the Unit are strongly erosive, whereas the interval around 120 m is more laterally extensive with a less erosive base. Both share similar dimensions and orientation, dipping more or less north. The upper IHS, however, has a basal cross-stratified interval interpreted as a basal channel lag, unlike the two lower units, which contain only inclined strata, suggesting the upper part developed in the more proximal part of the fluvial-tidal transition (Dalrymple & Choi, 2007).

In the eastern study area sandstone beds with tabular cross-bedding formed in energy conditions near the lower boundary for 2D dunes, typical for the lower to upper point bar in low-energy sandy meandering rivers (Martinius & van

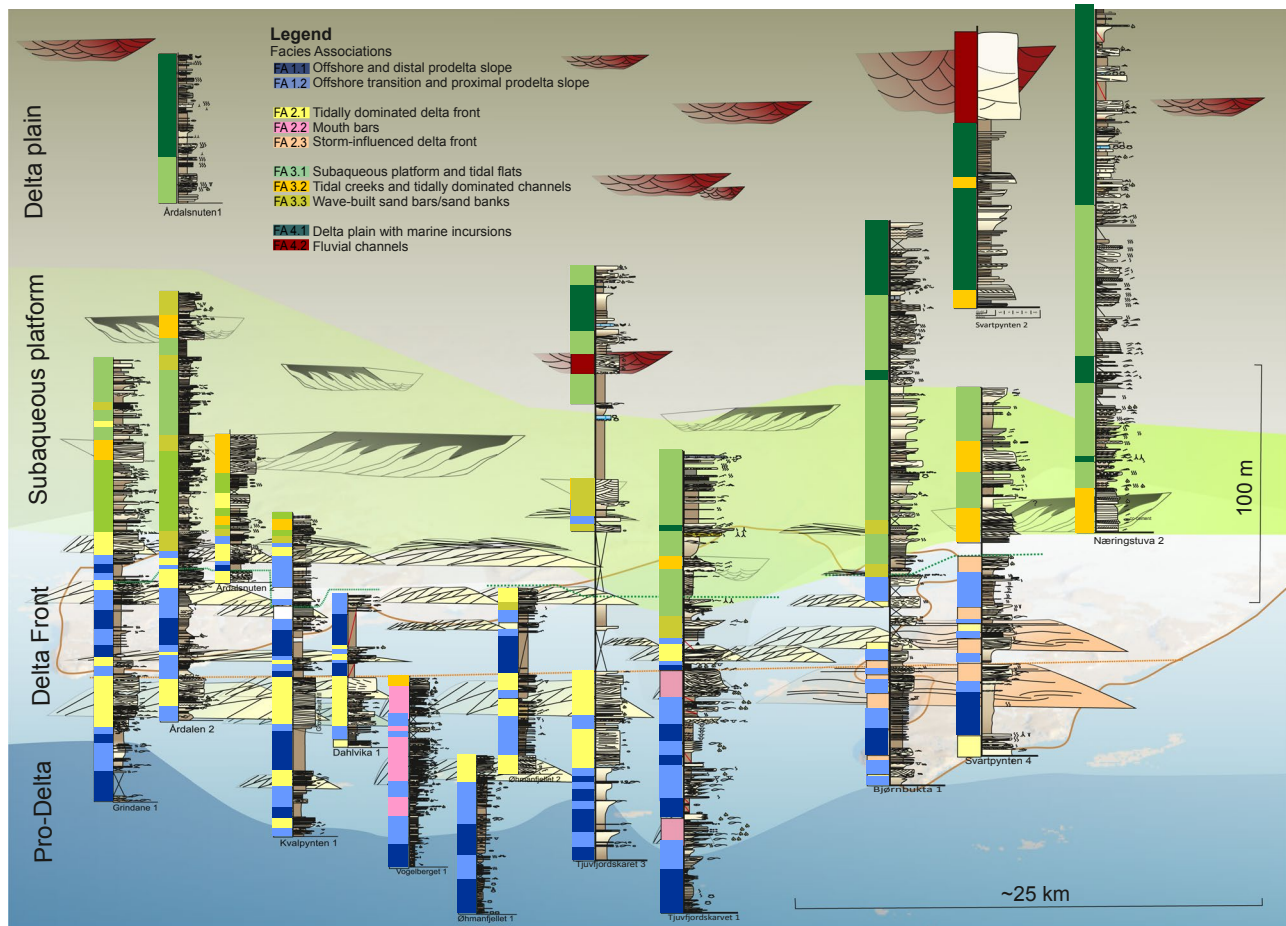


FIGURE 13 A summary figure showing the main logs across the whole study area (a transparent map underlays the logs to guide in relative horizontal location) with the interpreted facies associations shown in thick coloured stacks on the left of each log. The shaded background colour shows the overall transition from pro-delta through delta front across the subaqueous platform and into the delta plain. The cartoon-drawings of some of the main sandbody types found at various locations and sketched into the figure to show a generalized development of the type of sandbodies

den Berg, 2011). The eastern study area was probably dissected by a number of smaller creeks draining into the larger channels, such as those observed at Kvalpynten (Figure 6). The channel infill in the east study area changes from the strongly tidally influenced tabular cross-bedded fining upward units, to the massive trough cross-stratified sandstones incising the delta plain (Figure 10i–l), a development similar to that seen on Kvalpynten (Figure 10a). The channel sandbodies in both east and west are characterized by limited lateral accretion, with high depth-to-width ratios (Table 3). The symmetric orientation displayed in a north-south section indicates a westerly infill. They most likely represent fluvial distributary channels draining vegetated areas (Figure 12). The coarsest sands are confined to the fluvial channels, which appear narrower and straighter than the tidal/tidally dominated channels (Table 3). A flood-dominated tidal prism could confine coarse sediment up-river as the tidal wave becomes channelized and amplified upstream (Goodbred & Saito, 2012). The size of channels interpreted to be of fluvial origin is very similar to fluvial channels found on Hopen,

which is dominated by fluvial channels (Lord, Solvi, Klausen, & Mørk, 2014). Analysis of channels in the Snadd Formation reveals that proximal fluvial influenced channels reach up to 20 km width, decreasing to a few hundred metres in the distal delta plain (Klausen, Laursen, Ryseth, Gawthorpe, & Helland-Hansen, 2014). In light of this, observed features are interpreted as proximal fluvial channels which in turn connect to distal tidally dominated channels that widen across the subaqueous platform.

Sediment delivery is dominantly south-westward in the lowermost deposits of Unit 1 and 2, transitioning to more westward and north-westward in Unit 3 (Figure 11), in line with the general infill across Barents Shelf (Anell, Braathen, et al., 2014; Anell, Faleide, et al., 2016; Anell, Lecomte, et al., 2016; Glørstad-Clark et al., 2011). This complexity likely results from local infill patterns along an articulated coastline, accentuated by the low-stand, which promoted development of embayments and connected subsystems (Bhattacharya, 2006; Osmundsen et al., 2014). An overall westward-directed transport in Unit 3 probably also reflects

a new sediment provenance with the influx of a Northern Uraloid Sand, observed in zircon analysis of the De Geerdalen Formation and interpreted to be sourced from Taimyr and Severnaya Zemlya (Fleming et al., 2016). However, input from a more northerly Triassic source cannot be ruled out.

5 | DISCUSSION

Spectacular cliff exposures on Edgeøya, East Svalbard, offer a unique possibility to study the evolution of a delta front related to regional-scale progradation. The succession studied records a regression followed by a transgression and maximum flooding and then renewed highstand progradation. The Carnian age and prominence of the maximum flooding surface (MFS) suggests it is probably the equivalent of the Intra Carnian MFS observed in the seismic data in the SW Barents Sea (Klausen, Ryseth, Helland-Hansen, Gawthorpe, & Laursen, 2015).

The Triassic deposits record the passage of the seismic-scale clinoform system, which covered the entire western Barents Shelf (Anell, Midtkandal, & Braathen, 2014b; Glørstad-Clark et al., 2010; Riis et al., 2008; Rossi, Paterson, Helland-Hansen, Klausen, & Eide, 2019). The equivalent offshore formation of the De Geerdalen Formation is the Snadd Formation (Figure 2). Unlike the sand-rich subaqueous delta front on Edgeøya, the clinoforms in the Snadd Formation are generally muddy to silty, with sandstones confined mainly to channel bodies (Klausen et al., 2015).

The deltaic clinoforms on the Barents Shelf have been interpreted to be de-coupled from the coast (Klausen et al., 2015; Rossi et al., 2019). In the study area on Edgeøya, all indications also point towards a de-coupled system, with a sandy subaqueous delta front dominated by compound dunes separated from the coastline by an extensive subaqueous platform, in turn comprising subtidal deposits and occasional wave-build sandbodies. Even without such indices the degree of tidal influence alone would promote rapid subaqueous progradation physically separated from the shoreline (Patrino et al., 2015; Plink-Björklund, 2012), with waves and tidal currents limiting accommodation in the near-shore areas, similar to the Fly, Changjiang, Ganges–Brahmaputra and Amazon deltas (Cummings et al., 2015; Hori, Saito, Zhao, & Wang, 2002). Tidal currents are efficient agents in transporting sand long distances away from the shoreline (Rossi et al., 2016). Typically small-scale, 10–15 m high and partly subaerial clinoforms develop which are detached from larger 40–150 m subaqueous clinoforms, which tend to be long and gentle (Plink-Björklund, 2012). The subaqueous platform can extend for many kilometres in both width and length (Goodbred & Kuehl, 1999; Roberts & Sydow, 2003; Rossi & Steel, 2016; Swenson et al., 2005).

Wave- and tide-dominated depositional environments are often considered as two end-members, with the distinct sheltered heterolithic tidal flat succession in stark contrast to the exposed wave and storm generated deposits (Yang et al., 2005). Meanwhile it is apparent that complex interactions between wave, tide and fluvial processes over time and space can produce very variable deposits within a single system (Rossi & Steel, 2016). In the Havert Formation, one of the earliest prograding Triassic deposits on the southwest Barents Shelf, a mixed-energy influence on the deposits is appreciable with the tidal signature seen dominantly in near-shore proximal facies (Rossi et al., 2019). It has therefore been inferred that the tidal influence was not as strong as in, for example, the Jurassic deposits of the mid-Norwegian shelf (van Cappelle et al., 2017).

The deposits on Edgeøya show a high degree of tidal influence, but along depositional strike, contemporaneous fluvial-, wave- and tide-dominated deposits are observed in the delta front (Figures 12,13). This variability is interpreted to reflect changes in sediment influx, where the highest sedimentation rates led to preserved mouth bars, whereas tides generally redistributed sediment to form a compound dune field as seen in most of the western study area. The eastern study area is interpreted to reflect a setting more distant from the main fluvio-deltaic influx, which was subject to a higher degree of reworking by storms and waves (Fan, 2011; van Cappelle et al., 2017; Yang et al., 2005), common in tide-dominated systems (Morgan, 1970; Van Andel, 1967). Lower sediment influx also generates a narrower subaqueous platform and more limited dampening of the waves. The transgression, meanwhile, preserves more typical tidal sand-bodies also in the east, probably reflecting the classical tidal amplification associated with increased coastline complexity and formation of embayments (Boyd et al., 1992; Dalrymple, 2011). This is in stark contrast to the increased wave influence interpreted during back-stepping in the Early Carnian in the western Barents Shelf (Klausen, Ryseth, Helland-Hansen, & Gjelberg, 2016).

The subaqueous platform and lower delta plain record a largely tide-dominated setting with wave influence (Tw, *Sensu* Ainsworth, Vakarelov, & Nanson, 2011). These deposits are mud-rich and form another fine-grained depo-centre in addition to the pro-delta area (Plink-Björklund, 2012). When accommodation increases slowly, meandering tidal channels effectively rework the coastal area leaving no preserved tidal flat deposits (McIlroy et al., 2008). During more rapid accommodation generation, meander belts will be narrower with less tendency to amalgamate. The extensive preservation of subtidal flat deposits and isolated tidal channel bodies suggests a rapidly prograding system advancing across the Svalbard Platform. Rapid progradation across Svalbard during the late Triassic has previously been inferred to result from more limited accommodation, which promotes

accelerated progradation (Anell, Faleide, et al., 2016; Anell, Lecomte, et al., 2016).

The energy of the tidal wave increases where it is structurally constricted, either vertically or laterally (Cummings et al., 2006), which means that the highest tides are often found within restricted bays, funnels and embayments (Archer & Hubbard, 2003). Due to vertical confinement, the wider the shelf, the higher the tidal energy and therefore coastal systems >75 km wide, which included the Triassic coastline across the northern Barents Shelf, have a tendency to be tidally dominated (Ainsworth et al., 2011; Heap, Bryce, & Ryan, 2004; Klein & Ryer, 1978; Longhitano, Mellere, Steel, & Ainsworth, 2012; Redfield, 1958; Vakarelov, Ainsworth, & MacEachern, 2012). The wide subaqueous platform additionally attenuates wave action due to enhanced basal friction (Choi et al., 2004; Cummings et al., 2015; Feldman & Demko, 2015). Whereas tidal amplification is inherently complex (Archer & Hubbard, 2003; Cummings et al., 2006; Klein & Ryer, 1978; Rossi et al., 2016) and dependant on several factors, it stands to reason that the increased degree of tidal influence apparent at Edgeøya compared to the SW Barents Shelf, is the effect of a shallower setting, whereby wave energy was attenuated, and tidal energy was further amplified. Amplification is suggested to have increased sand-transport away from the coast, thus explaining the increased sand content in shallow marine deposits compared to the offshore Snadd Formation. Both the Snadd and De Geerdalen formations are, however, characterized by very limited sediment bypass to a deep marine setting, despite being classified as supply-dominated (Carvajal, Steel, & Petter, 2009; Klausen et al., 2015). The shallow angle of the prograding system likely inhibited gravity-driven processes, a setting which was also further enhanced across the structural high (Figure 12). The increased tidal influence and extensive preservation of tidal flat and tidal channel deposits suggest that the platform was elongated, and that across the structural high the distance between the subaqueous delta front and subaerial coastline increased.

The typical subdivision of deltas into wave-, tide- or fluvial-dominated is considered now to represent rather unique end-members of the system, and that many delta systems are actually affected by all three factors (Ainsworth et al., 2011; Bhattacharya, 2006; Olariu & Bhattacharya, 2006; Plink-Björklund, 2008; Rossi & Steel, 2016; Tanavsuu-Milkeviciene & Plink-Björklund, 2009; Vakarelov et al., 2012). Additionally the coexistence of wave and tide signals in a sedimentary system has been used to differentiate between regressive and transgressive cycles, since tidal amplification tends to occur when incised valleys are drowned (Legler et al., 2014). The interplay of tide and wave processes inferred at Edgeøya suggests deposition in a mesotidal to macrotidal setting. In macrotidal systems sediments are often organized in sandy bars in the shallow environment and compound dune fields in the

deeper areas (Longhitano et al., 2012). On the other hand, in mesotidal settings wave influence is much stronger, with formation of sand barriers intersected by tidal inlets, and ebb and tide deltas. With increasing tidal range barrier islands decrease in size and degenerate into scattered sand bank islands beyond a certain threshold (Davis & Flemming, 1995; Flemming, 2012; Oost & De Boer, 1994), and the deposits on Edgeøya likely reflect such a threshold setting in which scattered wave-built sand-bodies occur near the coastline (Figure 12).

6 | CONCLUSIONS

The study provides insight into the depositional environment and sandbody distribution in the Triassic De Geerdalen Formation on Edgeøya, Svalbard, documenting the effects of mixed-energy and tidal influence during shallowing on a wide shelf, and the effects of underlying topography on clinof orm development.

The increased degree of tidal influence apparent in the deposits on Edgeøya is inferred to result from amplification due to vertical constriction as the system prograded across a shallow platform. Further tidal amplification is also apparent within growth-faults where the tidal energy was structurally confined, and during transgression as a result of assumed increased coastline roughness and formation of embayments.

During passage onto the shallower Svalbard Platform, the development of shelf-prism (seismic) scale clinof orms was inhibited, and smaller-scale (delta-scale) intra-shelf clinof orms comprising a detached compound clinof orm system developed. The tidal amplification resulted in larger amounts of sand being transported to the subaqueous delta front. Tidal redistribution largely reworked mouth-bar deposits, which are only occasionally preserved. Areas with lower sediment input were subjected to increased amount of wave reworking, an effect which was likely increased due to the narrower shelf and less dampening of waves. In areas of higher sedimentation rates, an extensive lengthy subaqueous platform developed where waves were dampened and the vertical restriction further amplified the tidal signature. The preserved successions reflect highly bioturbated heterolithic tidal flat deposits. The platform was intersected by highly meandering tidal channels and smaller tidal creeks. The delta plain was incised by sand-rich, straighter and narrower fluvial distributary channels, with the tidal prism likely confining coarser deposits up-river.

ACKNOWLEDGEMENTS

We kindly thank our reviewers Tim Cullen, Albina Gilmullina and Ron Steel and editor Atle Rotevann, for helpful and constructive input. This study was funded by the

project 'Reconstructing the Triassic Northern Barents Shelf – Basin Infill Patterns Controlled by Gentle Sags and Faults' (Trias North: <http://www.mn.uio.no/triasnorth/>) under grant No. 234152 from the Research Council of Norway (RCN) and with financial support from Tullow Oil Norge, Lundin Norway, Equinor, Edison Norge and Dea Norge. We are thankful to everyone who was a part of the field-campaigns; Luca Blazic, Klaus Dittmers, Anna Dustira, Beyene Girma Haile, Helge Hellevang, Leif Bjørnar Henriksen, Berit Husteli, Arild Jørstad, Tore Grane Klausen (who is also thanked for contributing several great photos), Inger Laursen, Kristian Liland, Sean Mackie, Darki Matesic, Krzysztof Michaliski, Bjarte Rismyhr, Vidar Storvoll, Marta Woldengen and contributed to logging, photography and discussion. We thank Benjamin Dolva and Karin Ringdal (VOG Group, NORCE) for processing the virtual outcrop models, and extension of LIME software within the project framework.

PEER REVIEW

The peer review history for this article is available at <https://publons.com/publon/10.1111/bre.12482>.

DATA AVAILABILITY STATEMENT

The data that support the findings of this study are available from the corresponding author upon reasonable request. The photogrammetric model is now available on v3geo.com.

ORCID

Ingrid Anell  <https://orcid.org/0000-0001-6489-5075>
 Valentin Zuchuat  <https://orcid.org/0000-0002-2029-6422>
 Aleksandra Smyrak-Sikora  <https://orcid.org/0000-0001-9321-1269>
 Simon Buckley  <https://orcid.org/0000-0001-8680-8286>
 Ivar Midtkandal  <https://orcid.org/0000-0002-4507-288X>
 Kei Ogata  <https://orcid.org/0000-0002-4978-2854>
 Alvar Braathen  <https://orcid.org/0000-0002-0869-249X>

REFERENCES

- Ahmed, S., Bhattacharya, J. P., Garza, D. E., & Li, Y. (2014). Facies architecture and stratigraphic evolution of a river-dominated delta front, Turonian Ferron Sandstone, Utah, U.S.A. *Journal of Sedimentary Research*, 84(2), 97–121. <https://doi.org/10.2110/jsr.2014.6>
- Ainsworth, R. B., Vakarelov, B. K., & Nanson, R. A. (2011). Dynamic spatial and temporal prediction of changes in depositional processes on clastic shorelines: Toward improved subsurface uncertainty reduction and management. *American Association of Petroleum Geologists Bulletin*, 95, 267–297. <https://doi.org/10.1306/06301010036>
- Allen, P. A., & Honewood, P. (1984). Evolution and mechanics of a Miocene tidal sandwave. *Sedimentology*, 31, 63–81. <https://doi.org/10.1111/j.1365-3091.1984.tb00723.x>
- Anell, I., Braathen, A., & Olausson, S. (2014). The triassic-early jurassic of the northern barents shelf: A regional understanding of the longyearbyen CO2 reservoir. *Norsk Geologisk Tidsskrift*, 94, 83–98.
- Anell, I., Faleide, J. I., & Braathen, A. (2016). Regional tectono-sedimentary development of the highs and basins of the northwestern Barents shelf. *Norsk Geologisk Tidsskrift*, 96, 27–41. <https://doi.org/10.17850/njg96-1-04>
- Anell, I., Lecomte, I., Braathen, A., & Buckley, S. J. (2016). Synthetic seismic illumination of small-scale growth faults, paralic deposits and low-angle clinoforms: A case study of the Triassic successions on Edgeøya, NW Barents Shelf. *Marine and Petroleum Geology*, 77, 625–639. <https://doi.org/10.1016/j.marpetgeo.2016.07.005>
- Anell, I., & Midtkandal, I. (2017). The quantifiable clinotherm – types, shapes and geometric relationships in the Plio-Pleistocene Giant Foresets Formation, Taranaki Basin, New Zealand. *Basin Research*, 29, 277–297. <https://doi.org/10.1111/bre.12149>
- Anell, I., Midtkandal, I., & Braathen, A. (2014). Trajectory analysis and inferences on geometric relationships of an Early Triassic prograding clinoform succession on the northern Barents Shelf. *Marine and Petroleum Geology*, 54, 167–179. <https://doi.org/10.1016/j.marpetgeo.2014.03.005>
- Archer, A. W., & Hubbard, M. S. (2003). Highest tides of the world. *Special Paper of the Geological Society of America*, 370, 151–174. <https://doi.org/10.1130/0-8137-2370-1.151>
- Ashley, G. M., Southard, J. B., & Boothroyd, J. C. (1982). Deposition of climbing ripple beds: A flume simulation. *Sedimentology*, 29, 67–79. <https://doi.org/10.1111/j.1365-3091.1982.tb01709.x>
- Ávila, S. P., Ramalho, R. S., Habermann, J. M., Quartau, R., Kroh, A., Berning, B., ... Madeira, J. (2015). Palaeoecology, taphonomy, and preservation of a lower Pliocene shell bed (coquina) from a volcanic oceanic island (Santa Maria Island, Azores). *Palaeogeography, Palaeoclimatology, Palaeoecology*, 430, 57–73. <https://doi.org/10.1016/j.palaeo.2015.04.015>
- Baas, J. H., Best, J. L., & Peakall, J. (2016). Predicting bedforms and primary current stratification in cohesive mixtures of mud and sand. *Journal of the Geological Society of London*, 173, 12–45. <https://doi.org/10.1144/jgs2015-024>
- Basilici, G. (1997). Sedimentary facies in an extensional and deep-lacustrine depositional system: The Pliocene Tiberino Basin, Central Italy. *Sediment. Geol.*, 109, 73–94. [https://doi.org/10.1016/S0037-0738\(96\)00056-5](https://doi.org/10.1016/S0037-0738(96)00056-5)
- Bhattacharya, J. P. (2006). Deltas. In H. Posamentier, & R. Walker (Eds.), *Facies models revisited* (pp. 237–292). Tulsa, Oklahoma: SEPM Special Publication.
- Bhattacharya, J. P., & MacEachern, J. A. (2009). Hyperpycnal rivers and prodeltaic shelves in the cretaceous seaway of North America. *Journal of Sedimentary Research*, 79, 184–209. <https://doi.org/10.2110/jsr.2009.026>
- Bown, T. M., & Kraus, M. J. (1993). Time-Stratigraphic Reconstruction and Integration of Paleopedologic, Sedimentologic, and Biotic Events (Willwood Formation, Lower Eocene, Northwest Wyoming, U.S.A.). *Palaios*, 1993, 68–80. <https://doi.org/10.2307/3515222>
- Boyd, R., Dalrymple, R., & Zaitlin, B. A. (1992). Classification of clastic coastal depositional environments. *Sedimentary Geology*, 80, 139–150. [https://doi.org/10.1016/0037-0738\(92\)90037-R](https://doi.org/10.1016/0037-0738(92)90037-R)
- Braathen, A., Maher, H. J., Haabet, T. E., Kristensen, S. E., Tørrudbakken, B. O., & Worsley, D. (1999). Caledonian thrusting on Bjørnøya: Implications for Palaeozoic and Mesozoic tectonism of the western Barents Shelf. *Norsk Geologisk Tidsskrift*, 79, 57–68.
- Braathen, A., Osmundsen, P. T., Maher, H., & Ganerød, M. (2018). The Keisarhjelmen detachment records Silurian-Devonian extensional collapse in Northern Svalbard. *Terra Nova*, 30(1), 34–39. <https://doi.org/10.1111/ter.12305>

- Buckley, S. J., Howell, J. A., Enge, H. D., & Kurz, T. H. (2008). Terrestrial laser scanning in geology: Data acquisition, processing and accuracy considerations. *Journal of the Geological Society of London*, *165*, 625–638. <https://doi.org/10.1144/0016-76492007-100>
- Buckley, S. J., Ringdal, K., Naumann, N., Dolva, B., Kurz, T. H., Howell, J. A., & Dewez, T. J. (2019). LIME: Software for 3-D visualization, interpretation, and communication of virtual geoscience models. *Geosphere*, *15*, 222–235. <https://doi.org/10.1130/GES02002.1>
- Bullimore, S., Henriksen, S., Liestøl, F. M., & Helland-Hansen, W. (2005). Clinoforms stacking patterns, shelf-edge trajectories and facies associations in Tertiary coastal deltas, offshore Norway: Implications for the prediction of lithology in prograding systems. *Norwegian Journal of Geology*, *85*, 167–187.
- Carvajal, C., Steel, R., & Petter, A. (2009). Sediment supply: The main driver of shelf-margin growth. *Earth-Science Reviews*, *96*, 221–248. <https://doi.org/10.1016/j.earscirev.2009.06.008>
- Cheel, R. J., & Leckie, D. A. (1993). Hummocky cross stratification. In W. P. Wright (Ed.), *Sedimentology review* (Vol. 1, pp. 103–122). Oxford, UK: Blackwell.
- Choi, K. S., Dalrymple, R. W., Chun, S. S., & Kim, S.-P. (2004). Sedimentology of Modern, Inclined Heterolithic Stratification (IHS) in the Macrotidal Han River Delta, Korea. *Journal of Sedimentary Research*, *74*(5), 677–689. <https://doi.org/10.1306/030804740677>
- Cummings, D. I., Arnott, R. W. C., & Hart, B. S. (2006). Tidal signatures in a shelf-margin delta. *Geology*, *34*, 249–252. <https://doi.org/10.1130/G22078.1>
- Cummings, D. I., Dalrymple, R. W., Choi, K., & Jin, J. H. (2015). *The tide-dominated Han River Delta, Korea: Geomorphology, sedimentology, and stratigraphic architecture*, Amsterdam, Netherlands: Elsevier. <https://doi.org/10.1016/C2013-0-15362-7>
- Dallmann, W. K., Ohta, Y., Elvevold, S., & Blomeier, D. (2002). Bedrock map of Svalbard and Jan Mayen 1:750,000, with insert maps 1:250,000. Nor. Polarinstitutt Temakart No. 33.
- Dalrymple, R. W. (2010). Tidal depositional systems. In: N. James, & R. W. Dalrymple (Eds.), *Facies models 4* (pp. 201–231). St Johns, Canada: Geological Association of Canada.
- Dalrymple, R. W. (2011). Incised valleys in time and space: An introduction to the volume and an examination of the controls on valley formation and filling. Special Publications of SEPM 85, 5–12. <https://doi.org/10.2110/pec.06.85.0005>
- Dalrymple, R. W., & Choi, K. (2007). Morphologic and facies trends through the fluvial–marine transition in tide-dominated depositional systems: A schematic framework for environmental and sequence-stratigraphic interpretation. *Earth-Science Reviews*, *81*, 135–174. <https://doi.org/10.1016/j.earscirev.2006.10.002>
- Dalrymple, R. W., Knight, R. J., & Lambiase, J. J. (1978). Bedforms and their hydraulic stability relationships in a tidal environment, Bay of Fundy, Canada. *Nature*, *275*, 100–104. <https://doi.org/10.1038/275100a0>
- Dashtgard, S. E. (2011). Linking invertebrate burrow distributions (neolithology) to physicochemical stresses on a sandy tidal flat: Implications for the rock record. *Sedimentology*, *58*, 1303–1325. <https://doi.org/10.1111/j.1365-3091.2010.01210.x>
- Davis, R. A. (2010). Tidal signatures and their preservation potential in stratigraphic sequences. R. A. Davis & R. W. Dalrymple In: *Principles of tidal sedimentology* (pp. 35–55). Dordrecht: Springer. https://doi.org/10.1007/978-94-007-0123-6_3
- Davis, R. A., & Flemming, B. W. (1995). Stratigraphy of a combined Wave- and Tide-Dominated Intertidal Sand Body: Martens Plate, East Frisian Wadden Sea, Germany. B. W. Flemming & A. Bartholoma In: *Tidal signatures in modern and ancient sediments*, Hoboken, NJ: Wiley-Blackwell. <https://doi.org/10.1002/9781444304138.ch8>
- Desjardins, P., Buatois, L., & Mangano, M. G. (2012). Tidal flats and subtidal sand bodies. *Trace Fossils as Indicators of Sedimentary Environments, Developments in Sedimentology*, *64*, 529–561.
- Dumas, S., & Arnott, R. W. C. (2006). Origin of hummocky and swaley cross-stratification - The controlling influence of unidirectional current strength and aggradation rate. *Geology*, *34*, 1073–1076. <https://doi.org/10.1130/G22930A.1>
- Edwards, M. B. (1976). Growth faults in upper Triassic deltaic sediments, Svalbard. *AAPG Bulletin*, *60*, 341–355. <https://doi.org/10.1306/83D923BB-16C7-11D7-8645000102C1865D>
- Elliott, T. (1974). Interdistributary bay sequences and their genesis. *Sedimentology*, *21*(4), 611–622.
- Faleide, J. I., Pease, V., Curtis, M., Klitzke, P., Minakov, A., Scheck-Wenderoth, M., ... Zayonchek, A. (2018). Tectonic implications of the lithospheric structure across the Barents and Kara shelves. In: V. Pease, & B. J. Coakley (Eds.), *Circum-Arctic Lithosphere Evolution*, Geological Society of London Special Publications, (Vol. 460, 285–314). London, UK: Geological Society. <https://doi.org/10.1144/SP460.18>
- Faleide, J. I., Tsikalas, F., Breivik, A. J., Mjelde, R., Ritzmann, O., Engen, Ø., ... Eldholm, O. (2008). Structure and evolution of the continental margin off Norway and the Barents Sea. *Episodes*, *31*, 82–91. <https://doi.org/10.18814/epiugs/2008/v31i1/012>
- Fan, D. (2011). Open-coast tidal flats. R. A. Davis & R. W. Dalrymple In: *Principles of Tidal Sedimentology* (pp. 187–229). Dordrecht, Netherlands: Springer. https://doi.org/10.1007/978-94-007-0123-6_9
- Feldman, H., & Demko, T. (2015). Recognition and Prediction of Petroleum reservoirs in the Fluvial-Tidal Transition. In P. J. Ashworth, J. L. Best, & D. R. Parsons (Eds.), *Fluvial-tidal sedimentology* (pp. 483–519). Amsterdam: Elsevier.
- Fielding, C. R. (2006). Upper flow regime sheets, lenses and scour fills: Extending the range of architectural elements for fluvial sediment bodies. *Sedimentary Geology*, *190*, 227–240. <https://doi.org/10.1016/j.sedgeo.2006.05.009>
- Fleming, E. J., Flowerdew, M. J., Smyth, H. R., Scott, R. A., Morton, A. C., Omma, J. E., ... Whitehouse, M. J. (2016). Provenance of Triassic sandstones on the southwest Barents Shelf and the implication for sediment dispersal patterns in northwest Pangaea. *Marine and Petroleum Geology*, *78*, 516–535. <https://doi.org/10.1016/j.marpetgeo.2016.10.005>
- Flemming, B. W. (2012). Siliciclastic back-barrier tidal flats. R. A. Davis & R. W. Dalrymple In: *Principles of tidal sedimentology* (pp. 231–267). Dordrecht, Netherlands: Springer. https://doi.org/10.1007/978-94-007-0123-6_10
- Gee, D. G., Bogolepova, O. K., & Lorenz, H. (2006). The Timanide, Caledonide and Uralide orogens in the Eurasian high Arctic, and relationships to the palaeo-continent Laurentia, Baltica and Siberia. In: D. G. Gee, & R. A. Stephenson (Eds.), *The geological society of London memoirs* (pp. 507–520). London. <https://doi.org/10.1144/GSL.MEM.2006.032.01.31>
- Gernigon, L., Brönnner, M., Roberts, D., Olesen, O., Nasuti, A., & Yamasaki, T. (2014). Crustal and basin evolution of the southwestern Barents Sea: From Caledonian orogeny to continental breakup. *Tectonics*, *33*, 347–373. <https://doi.org/10.1002/2013TC003439>
- Gingras, M. K., Pemberton, S. G., Saunders, T., & Clifton, H. E. (1999). The ichnology of modern and pleistocene brackish-water deposits at

- Willapa Bay, Washington: Variability in estuarine settings. *Palaios*, 14, 352–374. <https://doi.org/10.2307/3515462>
- Gingras, M. K., Pemberton, S. G., & Smith, M. (2015). Bioturbation: Reworking sediments for better or worse. *Oilfield Review*, 26, 46–58.
- Glørstad-Clark, E., Birkeland, E. P., Nystuen, J. P., Faleide, J. I., & Midtkandal, I. (2011). Triassic platform-margin deltas in the western Barents Sea. *Marine and Petroleum Geology*, 28, 1294–1314. <https://doi.org/10.1016/j.marpetgeo.2011.03.006>
- Glørstad-Clark, E., Faleide, J. I., Lundschieen, B. A., & Nystuen, J. P. (2010). Triassic seismic sequence stratigraphy and paleogeography of the western Barents Sea area. *Marine and Petroleum Geology*, 27, 1448–1475. <https://doi.org/10.1016/j.marpetgeo.2010.02.008>
- Goodbred, S. L., & Kuehl, S. A. (1999). Holocene and modern sediment budgets for the Ganges-Brahmaputra river system: Evidence for highstand dispersal to flood-plain, shelf, and deep-sea depocenters. *Geology*, 27, 559–562. [https://doi.org/10.1130/0091-7613\(1999\)027<0559:HAMSBF>2.3.CO;2](https://doi.org/10.1130/0091-7613(1999)027<0559:HAMSBF>2.3.CO;2)
- Goodbred, S. L., & Saito, Y. (2012). Tide-Dominated Deltas. R. A. Davis & R. W. Dalrymple In: *Principles of tidal sedimentology*, Dordrecht, Netherlands: Springer. https://doi.org/10.1007/978-94-007-0123-6_7
- Heap, A. D., Bryce, S., & Ryan, D. A. (2004). Facies evolution of Holocene estuaries and deltas: A large-sample statistical study from Australia. *Sedimentary Geology*, 168(1–2), 1–17. <https://doi.org/10.1016/j.sedgeo.2004.01.016>
- Helland-Hansen, W., & Hampson, G. J. (2009). Trajectory analysis: Concepts and applications. *Basin Research*, 21, 454–483. <https://doi.org/10.1111/j.1365-2117.2009.00425.x>
- Henriksen, E., Ryseth, A. E., Larssen, G. B., Heide, T., Ronning, K., Sollid, K., & Stoupakova, A. V. (2011). Chapter 10 Tectonostratigraphy of the greater Barents Sea: implications for petroleum systems. *Geological Society, London, Memoirs*, 35(1), 163–195. <https://doi.org/10.1144/M35.10>
- Hine, A. C. (1979). Mechanisms of berm development and resulting beach growth along a barrier spit complex. *Sedimentology*, 26, 333–351. <https://doi.org/10.1111/j.1365-3091.1979.tb00913.x>
- Hodgetts, D. (2013). Laser scanning and digital outcrop geology in the petroleum industry: A review. *Marine and Petroleum Geology*, 46, 335–354. <https://doi.org/10.1016/j.marpetgeo.2013.02.014>
- Hori, K., Saito, Y., Zhao, Q., & Wang, P. (2002). Architecture and evolution of the tide-dominated Changjiang (Yangtze) River delta, China. *Sedimentary Geology*, 146, 249–264. [https://doi.org/10.1016/S0037-0738\(01\)00122-1](https://doi.org/10.1016/S0037-0738(01)00122-1)
- Høy, T., & Lundschieen, B. A. (2011). Triassic deltaic sequences in the northern Barents Sea. In: A. M. Specer, A. F. Embry, D. L. Gautier, A. V. Stoupakova, & K. Sørensen (Eds.), *Geological society, London, memoirs* (pp. 249–260). London. <https://doi.org/10.1144/M35.15>
- Hughes, Z. J. (2012). Tidal channels on tidal flats and marshes. In R. A. Davis, & R. W. Dalrymple (Eds.), *Principles of Tidal Sedimentology*, Dordrecht, Netherlands: Springer.
- Jackson, M. D., Hampson, G. J., & Sech, R. P. (2009). Three-dimensional modeling of a shoreface-shelf parasequence reservoir analog: Part 2. Geologic controls on fluid flow and hydrocarbon recovery. *American Association of Petroleum Geologists Bulletin*, 93, 1155–1181. <https://doi.org/10.1306/05110908145>
- Jelby, M. E., Grundvåg, S.-A., Helland-Hansen, W., Olausson, S., & Stemmerik, L. (2017). *Basin-scale facies model of spectacular storm deposits in the High Arctic*. Copenhagen: Geological Society of Denmark Annual Meeting.
- Johannessen, E. P., & Steel, R. J. (2005). Shelf-margin clinoforms and prediction of deep-water sands. *Basin Research*, 15, 521–550. <https://doi.org/10.1111/j.1365-2117.2005.00278.x>
- Johansen, S. E., Ostist, B. K., Birkeland, Ø., Fedorovsky, Y. F., Martirosjan, V. N., Brunn Christensen, O., ... Margulis, L. S. (1993). *Hydrocarbon potential in the Barents Sea region: Play distribution and potential*. Elsevier, Amsterdam: Arctic Geology and Petroleum Potential.
- Johansson, Å., Gee, D. G., Larionov, A. N., Ohta, Y., & Tebenkov, A. M. (2005). Grenvillian and Caledonian evolution of eastern Svalbard—a tale of two orogenies. *Terra Nova*, 17, 317–325. <https://doi.org/10.1111/j.1365-3121.2005.00616.x>
- Klausen, T. G., Laursen, I., Ryseth, A. E., Gawthorpe, R., & Helland-Hansen, W. (2014). Spatial and temporal changes in geometries of fluvial channel bodies from the triassic snadd formation of offshore Norway. *Journal of Sedimentary Research*, 84, 567–585. <https://doi.org/10.2110/jsr.2014.47>
- Klausen, T. G., & Mørk, A. (2014). The upper triassic paralic deposits of the De Geerdalen formation on Hopen: Outcrop analog to the sub-surface Snadd formation in the Barents sea. *American Association of Petroleum Geologists Bulletin*, 98(10), 1911–1941. <https://doi.org/10.1306/02191413064>
- Klausen, T. G., Ryseth, A. E., Helland-Hansen, W., Gawthorpe, R., & Laursen, I. (2015). Regional development and sequence stratigraphy of the Middle to Late Triassic Snadd Formation, Norwegian Barents Sea. *Marine and Petroleum Geology*, 62, 102–122. <https://doi.org/10.1016/j.marpetgeo.2015.02.004>
- Klausen, T. G., Ryseth, A. E., Helland-Hansen, W., & Gjelberg, H. G. (2016). Progradational and backstepping shoreface deposits in the Ladinian to Early Norian Snadd Formation of the Barents Sea. *Sedimentology*, 63, 893–916. <https://doi.org/10.1111/sed.12242>
- Klein, G. D., & Ryer, T. A. (1978). Tidal circulation patterns in Precambrian, Paleozoic, and Cretaceous epeiric and mioclinal shelf seas. *Geological Society of America Bulletin*, 89, 1050–1058. [https://doi.org/10.1130/0016-7606\(1978\)89<1050:TCPIP>2.0.CO;2](https://doi.org/10.1130/0016-7606(1978)89<1050:TCPIP>2.0.CO;2)
- Kraus, M. J. (1999). Paleosols in clastic sedimentary rocks: Their geologic applications. *Earth-Science Reviews*, 47(1–2), 41–70. [https://doi.org/10.1016/S0012-8252\(99\)00026-4](https://doi.org/10.1016/S0012-8252(99)00026-4)
- Kuehl, S. A., Levy, B. M., Moore, W. S., & Allison, M. A. (1997). Subaqueous delta of the Ganges-Brahmaputra river system. *Marine Geology*, 144, 81–96. [https://doi.org/10.1016/S0025-3227\(97\)00075-3](https://doi.org/10.1016/S0025-3227(97)00075-3)
- Kurcinka, C., Dalrymple, R. W., & Gugliotta, M. (2018). Facies and architecture of river-dominated to tide-influenced mouth bars in the lower Lajas Formation (Jurassic), Argentina. *American Association of Petroleum Geologists Bulletin*, 102, 885–912. <https://doi.org/10.1306/0609171618917155>
- Legler, B., Hampson, G. J., Jackson, C.-A.-L., Johnson, H. D., Massart, B. Y. G., Sarginson, M., & Ravnas, R. (2014). Facies relationships and stratigraphic architecture of distal, mixed tide- and wave-influenced deltaic deposits: Lower Sego Sandstone, Western Colorado, U.S.A. *Journal of Sedimentary Research*, 84, 605–625. <https://doi.org/10.2110/jsr.2014.49>
- Longhitano, S. G., Mellere, D., Steel, R. J., & Ainsworth, R. B. (2012). Tidal depositional systems in the rock record: A review and new insights. *Sedimentary Geology*, 279, 2–22. <https://doi.org/10.1016/j.sedgeo.2012.03.024>
- Lord, G. S., Solvi, K. H., Klausen, T. G., & Mørk, A. (2014). Triassic channel bodies on Hopen, Svalbard: Their facies, stratigraphic

- significance and spatial distribution. *Norwegian Petroleum Directorate Bulletin*, 11, 41–59.
- MacEachern, J. A., & Bann, K. (2008). The role of ichnology in refining shallow marine facies models. In G. J. Hampson, R. J. Steel, P. M. Burgess, & R. W. Dalrymple (Eds.), *Recent advances in models of siliciclastic shallow-marine stratigraphy* (pp. 73–116). Tulsa, OK: SEPM Special Publications 90.
- Mángano, M. G., & Buatois, L. A. (2008). Ichnology of Carboniferous tide-influenced environments and tidal flat variability in the North American Midcontinent. *Geological Society, London, Special Publications*, 228(1), 157–178. <https://doi.org/10.1144/gsl.sp.2004.228.01.09>
- Martini, I., & Sandrelli, F. (2015). Facies analysis of a pliocene river-dominated deltaic succession (Siena Basin, Italy): Implications for the formation and infilling of terminal distributary channels. *Sedimentology*, 62, 234–265. <https://doi.org/10.1111/sed.12147>
- Martinius, A. W., Fustic, M., Garner, D. L., Jablonski, B., Strobl, R. S., MacEachern, J. A., & Dashtgard, S. E. (2017). Reservoir characterization and multiscale heterogeneity modeling of inclined heterolithic strata for bitumen-production forecasting, McMurray Formation, Corner, Alberta, Canada. *Marine and Petroleum Geology*, 82, 336–361. <https://doi.org/10.1016/j.marpetgeo.2017.02.003>
- Martinius, A. W., & van den Berg, J. H. (2011). *Atlas of sedimentary structures in estuarine and tidally-influenced river deposits of the Rhine-Meuse-Scheldt system*. Houten: EAGE Publications.
- Massari, F. (1996). Upper-flow-regime stratification types on steep-face, coarse-grained, gilbert-type progradational wedges (Pleistocene, Southern Italy). *Journal of Sedimentary Research*, 66(2), 364–375. <https://doi.org/10.1306/D426834C-2B26-11D7-8648000102C1865D>
- McIlroy, D., Flint, S., Howell, J. A., & Timms, N. (2008). Sedimentology of the tide-dominated Jurassic Lajas Formation, Neuquén Basin, Argentina. *Geological Society, London, Special Publications*, 252(1), 83–107. <https://doi.org/10.1144/GSL.SP.2005.252.01.05>
- McKerrow, W. S., Mac Niocaill, C., & Dewey, J. F. (2000). The caledoniano orogeny redefined. *Journal of the Geological Society*, 157(6), 1149–1154. <https://doi.org/10.1144/jgs.157.6.1149>
- Miall, A. D. (Ed.) (2016). *Facies analysis. In Stratigraphy: A modern synthesis* (pp. 77–159). Cham, Switzerland: Springer International Publishing. ISBN: 978-3-319-24302-3.
- Morgan, J. P. (1970). Depositional products and processes in the deltaic environment. In: J. P. Morgan, & R. H. Shaver (Eds.), *Deltaic sedimentation, modern and ancient* (vol. 15, pp. 31–47). Tulsa, OK: SEPM Special Publications. <https://doi.org/10.2110/pec.70.11.0031>
- Mørk, A., Dallmann, W. K., Dypvik, H., Johannesen, E. P., Larssen, G. B., Nagy, J., ... Worsley, D. (1999). Mesozoic lithostratigraphy. In W. K. Dallmann (Ed.), *Lithostratigraphic Lexicon of svalbard, review and recommendations for nomenclature use review and recommendations for nomenclature use*. Upper palaeozoic to quaternary bedrock (pp. 127–214). Tromsø, Norway: Norwegian Polar Institute.
- Moslow, T. F., & Pemberton, S. G. (1988). An integrated approach to the sedimentological analysis of some lower Cretaceous shoreface and delta front sandstone sequences. In D. J. James, & D. A. Leckie (Eds.), *Sequences, Stratigraphy, Sedimentology: Surface and Subsurface* (pp. 373–386). Alberta, Canada: Canadian Society of Petroleum Geologists memoir 15.
- Mueller, S., Veld, H., Nagy, J., & Kürschner, W. M. (2014). Depositional history of the upper triassic kapp toscana group on svalbard, Norway, inferred from palynofacies analysis and organic geochemistry. *Sedimentary Geology*, 310, 16–29. <https://doi.org/10.1016/j.sedgeo.2014.06.003>
- Niederoda, A. W., Swift, D. J. P., Hopkins, T. S., & Ma, C. M. (1984). Shoreface morphodynamics on wave-dominated coasts. *Marine Geology*, 60, 331–354. [https://doi.org/10.1016/S0070-4571\(08\)70153-5](https://doi.org/10.1016/S0070-4571(08)70153-5)
- Nio, S. D., & Yang, C. S. (1991). Sea-level fluctuations and the geometric variability of tide-dominated sandbodies. *Sedimentary Geology*, 70(2-4), 161–193. [https://doi.org/10.1016/0037-0738\(91\)90140-9](https://doi.org/10.1016/0037-0738(91)90140-9)
- Nøttvedt, A., Cecchi, M., Gjelberg, J. G., Kristensen, S. E., Lønøy, A., Rasmussen, A., ... van Veen, P. M. (1993). Svalbard-Barents Sea correlation: A short review. *Norwegian Petroleum Society Special Publications*, 2, 363–375. <https://doi.org/10.1016/B978-0-444-88943-0.50027-7>
- Ogata, K., Mulrooney, M. J., Braathen, A., Maher, H., Osmundsen, P. T., Anell, I., ... Balsamo, F. (2018). Architecture, deformation style and petrophysical properties of growth fault systems: The Late Triassic deltaic succession of southern Edgeøya (East Svalbard). *Basin Research*, 30, 1042–1073. <https://doi.org/10.1111/bre.12296>
- Olariu, C., & Bhattacharya, J. P. (2006). Terminal distributary channels and delta front architecture of river-dominated delta systems. *Journal of Sedimentary Research*, 76, 212–233. <https://doi.org/10.2110/jsr.2006.026>
- Olariu, C., Steel, R. J., Dalrymple, R. W., & Gingras, M. K. (2012). Tidal dunes versus tidal bars: The sedimentological and architectural characteristics of compound dunes in a tidal seaway, the lower Baronia Sandstone (Lower Eocene), Ager Basin, Spain. *Sedimentary Geology*, 279, 134–155.
- Olariu, C., Steel, R. J., & Petter, A. L. (2010). Delta-front hyperpynal bed geometry and implications for reservoir modeling: Cretaceous Panther Tongue delta, Book Cliffs, Utah. *AAPG Bulletin*, 94, 819–845. <https://doi.org/10.1306/11020909072>
- Oost, A. P. P., & De Boer, P. L. L. (1994). Sedimentology and development of barrier islands, ebb-tidal deltas, inlets and backbarrier areas of the Dutch Wadden Sea. *Senckenbergiana Maritima*, 24, 65–115.
- Osmundsen, P. T., Braathen, A., Rød, R. S., & Hynne, I. (2014). Styles of normal faulting and fault-controlled deposition in the Triassic of Hopen and Edgeøya, Svalbard. *Norwegian Petroleum Directorate Bulletin*, 11, 61–79.
- Otvos, E. G. (2000). Beach ridges - definitions and significance. *Geomorphology*, 32, 83–108. [https://doi.org/10.1016/S0169-555X\(99\)00075-6](https://doi.org/10.1016/S0169-555X(99)00075-6)
- Owen, G. (1987). Deformation processes in unconsolidated unconsolidated sands. *Geological Society, London, Special Publications*, 29(1), 11–24. <https://doi.org/10.1144/GSL.SP.1987.029.01.02>
- Paterson, N. W., & Mangerud, G. (2017). Palynology and depositional environments of the Middle–Late Triassic (Anisian–Rhaetian) Kobbe, Snadd and Fruholmen formations, southern Barents Sea, Arctic Norway. *Marine and Petroleum Geology*, 86, 304–324.
- Patruno, S., Hampson, G. J., & Jackson, C. A. L. (2015). Quantitative characterisation of deltaic and subaqueous clinoforms. *Earth Science Rev.*, 142, 79–119. <https://doi.org/10.1016/j.earscirev.2015.01.004>
- Patruno, S., Hampson, G. J., Jackson, C. A., & Dreyer, T. (2015). Clinoform geometry, geomorphology, facies character and stratigraphic architecture of a sand-rich subaqueous delta: Jurassic Sognefjord Formation, offshore Norway. *Sedimentology*, 62, 350–388. <https://doi.org/10.1111/sed.12153>

- Peters, S. E., & Loss, D. P. (2012). Storm and fair-weather wave base: A relevant distinction? *Geology*, *40*(6), 511–514. <https://doi.org/10.1130/G32791.1>
- Petter, A. L., & Steel, R. J. (2006). Hyperpycnal flow variability and slope organization on an Eocene shelf margin, Central Basin, Spitsbergen. *American Association of Petroleum Geologists Bulletin*, *90*(10), 1451–1472. <https://doi.org/10.1306/04240605144>
- Pickering, K., Stow, D., Watson, M., & Hiscott, R. (1986). Deep-water facies, processes and models: A review and classification scheme for modern and ancient sediments. *Earth-Science Reviews*, *23*, 75–174. [https://doi.org/10.1016/0012-8252\(86\)90001-2](https://doi.org/10.1016/0012-8252(86)90001-2)
- Pirmez, C., Pratson, L. F., & Steckler, M. S. (1998). Clinof orm development by advection-diffusion of suspended sediment: Modeling and comparison to natural systems. *Journal of Geophysical Research: Solid Earth*, *103*, 24141–24157. <https://doi.org/10.1029/98JB01516>
- Plink-Björklund, P. (2008). Wave-to-tide facies change in a Campanian Shoreline Complex, Chimney Rock Tongue, Wyoming-Utah, U.S.A. In G. J. Hampson, R. J. Steel, P. M. Burgess, & R. W. Dalrymple (Eds.), *Recent advances in models of siliciclastic shallow-marine stratigraphy* (pp. 265–291). Tulsa, OK: SEPM Special Publications 90.
- Plink-Björklund, P. (2012). Effects of tides on deltaic deposition: Causes and responses. *Sedimentary Geology*, *297*, 107–133. <https://doi.org/10.1016/j.sedgeo.2011.07.006>
- Plink-Björklund, P., Mellere, D., & Steel, R. J. (2001). Turbidite variability and architecture of sand-prone, deep-water slopes: Eocene clinof orms in the Central Basin, Spitsbergen. *Journal of Sedimentary Research*, *71*(6), 895–912. <https://doi.org/10.1306/030501710895>
- Plint, A. G., & Wadsworth, J. A. (2003). Sedimentology and palaeogeomorphology of four large valley systems incising delta plains, western Canada Foreland Basin: Implications for mid-Cretaceous sea-level changes. *Sedimentology*, *50*(6), 1147–1186. <https://doi.org/10.1111/j.1365-3091.2003.00599.x>
- Quin, J. G. (2011). Is most hummocky cross-stratification formed by large-scale ripples? *Sedimentology*, *58*, 1414–1433. <https://doi.org/10.1111/j.1365-3091.2010.01219.x>
- Redfield, A. C. (1958). The influence of the continental shelf on the tides of the Atlantic coast of the United States. *Journal of Marine Research*, *17*, 432–448.
- Riis, F., Lundschieen, B. A., Høy, T., Mørk, A., & Mørk, M.-B.-E. (2008). Evolution of the Triassic shelf in the northern Barents Sea region. *Polar Research*, *27*, 318–338.
- Rittersbacher, A., Howell, J. A., & Buckley, S. J. (2014). Analysis of fluvial architecture in the blackhawk formation, Wasatch Plateau, Utah, U.S.A., using large 3D photorealistic models. *Journal of Sedimentary Research*, *84*, 72–87. <https://doi.org/10.2110/jsr.2014.12>
- Roberts, H. H., & Sydow, J. (2003). Late Quaternary stratigraphy and sedimentology of the offshore Mahakam delta, east Kalimantan (Indonesia). In: F. H. Sidi, D. Nummedal, P. Imbert, D. H., & W. P. H (Eds.), *Tropical deltas of Southeast Asia* (vol. 76, pp. 125–145). Tulsa, OK: SEPM Special Publication. <https://doi.org/10.2110/pec.03.76.0125>
- Rossi, V. M., Kim, W., López, J. L., Edmonds, D., Geleynse, N., Olariu, C., ... Passalacqua, P. (2016). Impact of tidal currents on delta-channel deepening, stratigraphic architecture, and sediment bypass beyond the shoreline. *Geology*, *44*, 927–930. <https://doi.org/10.1130/G38334.1>
- Rossi, V. M., Paterson, N. W., Helland-Hansen, W., Klausen, T. G., & Eide, C. H. (2019). Mud-rich delta-scale compound clinof orms in the Triassic shelf of northern Pangea (Havert Formation, south-western Barents Sea). *Sedimentology*, *66*, 2234–2267. <https://doi.org/10.1111/sed.12598>
- Rossi, V. M., & Steel, R. J. (2016). The role of tidal, wave and river currents in the evolution of mixed-energy deltas: Example from the Lajas Formation (Argentina). *Sedimentology*, *63*, 824–864. <https://doi.org/10.1111/sed.12240>
- Sato, T., Taniguchi, K., Takagawa, T., & Masuda, F. (2011). Generation of tidal bedding in a circular flume experiment: Formation process and preservation potential of mud drapes. *Geo-Marine Letters*, *31*, 101–108. <https://doi.org/10.1007/s00367-010-0218-7>
- Schomacker, E. R., Kjemperud, A. V., Nystuen, J. P., & Jahren, J. S. (2010). Recognition and significance of sharp-based mouth-bar deposits in the Eocene Green River Formation, Uinta Basin, Utah. *Sedimentology*, *57*(4), 1069–1087. <https://doi.org/10.1111/j.1365-3091.2009.01136.x>
- Shen, Z., Törnqvist, T. E., Mauz, B., Chamberlain, E. L., Nijhuis, A. G., & Sandoval, L. (2015). Episodic overbank deposition as a dominant mechanism of floodplain and delta-plain aggradation. *Geology*, *43*, 875–878. <https://doi.org/10.1130/G36847.1>
- Sigmond, E. M. O. (1992). Bedrock map. Norway and adjacent ocean areas. Scale 1:3. Norges Geologiske Undersøkelse.
- Skogseid, J., Planke, S., Faleide, J. I., Pedersen, T., Eldholm, O., & Neverdal, F. (2000). NE Atlantic continental rifting and volcanic margin formation. In A. Nøttvedt (Ed.), *Dynamics of the Norwegian Margin*, Geological Society of London Special Publications (Vol. 167, pp. 295–326). London, UK: Lyell.
- Smelror, M., Petrov, O. V., Larssen, G. B., & Werner, S. C. (2009). *Geological history of the barents sea - atlas*. Trondheim: Geological Survey of Norway.
- Smyrak-Sikora, A., Osmundsen, P. T., Braathen, A., Ogata, K., Anell, I., Mulrooney, M. J., & Zuchuat, V. (2019). Architecture of growth basins in a tidally influenced, prodelta to delta front setting: The Triassic succession of Kvalpynten, East Svalbard. *Basin Research*. <https://doi.org/10.1111/bre.12410>
- Steel, R. J., & Olsen, T. (2002). Clinof orms, clinof orm trajectories and deepwater sands. In: J. M. Armentrout, & N. C. Rosen (Eds.), *Sequence stratigraphic models for exploration and production: Evolving methodology, emerging models and application histories* (pp. 367–381). Broken Arrow, OK: SEPM Special Publications 22.
- Stemmerik, L., & Worsley, D. (2005). 30 years on - Arctic Upper Palaeozoic stratigraphy, depositional evolution and hydrocarbon prospectivity. *Norsk Geologisk Forening*, *85*, 151.
- Swenson, J. B., Paola, C., Pratson, L., Voller, V. R., & Murray, A. B. (2005). Fluvial and marine controls on combined subaerial and subaqueous delta progradation: Morphodynamic modeling of compound clinof orm development. *Journal of Geophysical Research*, *110*, F02013. <https://doi.org/10.1029/2004JF000265>
- Tanavsuu-Milkeviciene, K., & Plink-Björklund, P. (2009). Recognizing tide-dominated versus tide-influenced deltas: Middle devonian strata of the baltic basin. *Journal of Sedimentary Research*, *79*, 887–905. <https://doi.org/10.2110/jsr.2009.096>
- Taylor, A. M., & Goldring, R. (1993). Description and analysis of bioturbation and ichnofabric. *Journal of the Geological Society of London*, *150*(1), 141–148. <https://doi.org/10.1144/gsjgs.150.1.0141>
- Teyssen, T. A. L. (1984). Sedimentology of the Minette oolitic ironstones of Luxembourg and Lorraine: A Jurassic subtidal sandwave complex. *Sedimentology*, *31*, 195–211. <https://doi.org/10.1111/j.1365-3091.1984.tb01959.x>

- Tye, R. S., & Coleman, J. M. (1989). Evolution of Atchafalaya lacustrine deltas, south-central Louisiana. *Sedimentary Geology*, 65, 95–112. [https://doi.org/10.1016/0037-0738\(89\)90008-0](https://doi.org/10.1016/0037-0738(89)90008-0)
- Vakarelov, B. K., Ainsworth, R. B., & MacEachern, J. A. (2012). Recognition of wave-dominated, tide-influenced shoreline systems in the rock record: Variations from a microtidal shoreline model. *Sedimentary Geology*, 279, 23–41. <https://doi.org/10.1016/j.sedgeo.2011.03.004>
- Van Andel, T. H. (1967). The orinoco delta. *SEPM Journal of Sedimentary Research*, 37, 297–310. <https://doi.org/10.1306/74d716c2-2b21-11d7-8648000102c1865d>
- van Cappelle, M., Ravnås, R., Hampson, G. J., & Johnson, H. D. (2017). Depositional evolution of a progradational to aggradational, mixed-influenced deltaic succession: Jurassic Tofte and Ile formations, southern Halten Terrace, offshore Norway. *Marine and Petroleum Geology*, 80, 1–22. <https://doi.org/10.1016/j.marpetgeo.2016.11.013>
- Venditti, J. G., Church, M., & Bennett, S. J. (2005). On the transition between 2D and 3D dunes. *Sedimentology*, 52(6), 1343–1359. <https://doi.org/10.1111/j.1365-3091.2005.00748.x>
- Vigran, O. S., Mangerud, G., Mørk, A., Worsley, D., & Hochuli, P. A. (2014). Palynology and geology of the Triassic succession of Svalbard and the Barents Sea. *Geological Survey of Norway Special Publication*, 14, 270.
- Visser, M. J. (1980). Neap- spring cycles reflected in Holocene subtidal large-scale bedform deposits: A preliminary note (Netherlands). *Geology*, 8, 543–546. [https://doi.org/10.1130/0091-7613\(1980\)8<543:NCRIHS>2.0.CO;2](https://doi.org/10.1130/0091-7613(1980)8<543:NCRIHS>2.0.CO;2)
- Wei, X., Steel, R. J., Ravnås, R., Jiang, Z., Olariu, C., & Li, Z. (2016). Variability of tidal signals in the Brent Delta Front: New observations on the Rannoch Formation, northern North Sea. *Sediment. Geol.*, 335, 166–179. <https://doi.org/10.1016/j.sedgeo.2016.02.012>
- Worsley, D. (2008). The post-Caledonian development of Svalbard and the western Barents Sea. *Polar Research*, 27, 298–317. <https://doi.org/10.1111/j.1751-8369.2008.00085.x>
- Yang, B. C., Dalrymple, R. W., & Chun, S. S. (2005). Sedimentation on a wave-dominated, open-coast tidal flat, south-western Korea: Summer tidal flat - Winter shoreface. *Sedimentology*, 52, 235–252. <https://doi.org/10.1111/j.1365-3091.2004.00692.x>

How to cite this article: Anell I, Zuchuat V, Röhnert AD, et al. Tidal amplification and along-strike process variability in a mixed-energy paralic system prograding onto a low accommodation shelf, Edgeøya, Svalbard. *Basin Res.* 2020;00:1–35. <https://doi.org/10.1111/bre.12482>